HHS Public Access

Author manuscript

ACS Appl Mater Interfaces. Author manuscript; available in PMC 2020 July 16.

Published in final edited form as:

ACS Appl Mater Interfaces. 2019 October 16; 11(41): 37381–37396. doi:10.1021/acsami.9b07053.

Triple PLGA/PCL scaffold modification including silver-impregnation, collagen-coating, and electrospinning significantly improve biocompatibility, antimicrobial, and osteogenic properties for oro-facial tissue regeneration

Yunzhu Qian[1], **Xuefeng Zhou**[2,*], **Feimin Zhang**[3], **Thomas G.H. Diekwisch**[4], **Xianghong Luan**[4,*], **Jianxin Yang**[1,*]

[1]Center of Stomatology, The Second Affiliated Hospital of Soochow University. Suzhou 215004, People's Republic of China

[2]State Key Laboratory of Bioelectronics, Jiangsu Key Laboratory for Biomaterials and Devices, School of Biological Science and Medical Engineering, Southeast University, Nanjing 210096, People's Republic of China

[3]Jiangsu Key Laboratory of Oral Diseases, Nanjing Medical University, Nanjing 210029, People's Republic of China

[4]Texas A&M Center for Craniofacial Research and Diagnosis, Dallas, Texas 75246, United States

Abstract

Biodegradable synthetic scaffolds hold great promise for oral and craniofacial guided tissue regeneration and bone regeneration. To overcome the limitations of current scaffold materials in terms of osteogenic and antimicrobial properties, we have developed a novel silver-modified/collagen-coated electrospun PLGA/PCL scaffold (PP-pDA-Ag-COL) with improved antimicrobial and osteogenic properties. Our novel scaffold was generated by electrospinning a basic PLGA/PCL matrix, followed by silver nanoparticle (AgNPs) impregnation via *in situ* reduction and polydopamine coating, and then coated by collagen I. The three intermediate materials involved in the fabrication of our scaffolds, PLGA/PCL (PP), PLGA/PCL-polydopamine (PP-pDA), and PLGA/PCL-polydopamine-Ag (PP-pDA-Ag) were used as control scaffolds. Scanning electron micrographs and mechanical testing indicated that the unique 3-dimensional structures with randomly-oriented nanofibrous electrospun-scaffold architectures, the elasticity modulus and the tensile strength were maintained after modifications. CCK-8 cell proliferation analysis demonstrated that the PP-pDA-Ag-COL scaffold was associated with higher MC3T3 proliferation rates than the three control scaffolds employed. Scanning electron and fluorescence light microscopy illustrated that PP-pDA-Ag-COL scaffolds significantly enhanced MC3T3 cell

[*]**Corresponding Author**: (J.Y) yangjx@gmail.com, (X.Z) zhouxuefeng@seu.edu.cn, (X.L) xianghong.luan@tamu.edu.

Author Contributions

Y.Q conceived the project and wrote the manuscript together with T.G.H.D. and. X.Z, X.L and J.Y designed the experiments. Y.Q and X.Z did the fabrication fabricated and characterization characterized of the scaffolds, and carried out MC3T3 cellular function tests on scaffolds including ALP, Western blot and RT-PCR under the instructions of F.Z, P.A and T.G.H.D.. SEM and CLSM images were captured by X.Z, and Y.Q performed antibacterial studies, and Y.Q and X.L did conduct the animal experiments. Y.Q is responsible for the statistical analysis. All authors reviewed the manuscript.

The authors declare no competing financial interest.

adhesion compared to the control scaffolds after 12h and 24h culture, in tandem with the highest β1 integrin expression levels, both at the mRNA level and the protein level. ALP activity, BMP2 and *RUNX2* expression levels of MC3T3 cells cultured on PP-pDA-Ag-COL scaffolds for 7 and 14 days were also significantly higher when compared to controls ($P < 0.001$). There was a wider antibacterial zone associated in PP-pDA-Ag-COL and PP-pDA-Ag scaffolds versus control scaffolds ($P < 0.05$), and bacterial fluorescence was reduced on the Ag-modified scaffolds after 24h inoculation against *S. aureus* and *S. mutans.* In a mouse periodontal disease model, the PP-pDA-Ag-COL scaffold enhanced alveolar bone regeneration (31.8%) and was effective for periodontitis treatment. These results demonstrate that our novel PP-pDA-Ag-COL scaffold enhanced biocompatibility, osteogenic and antibacterial properties and has therapeutic potential for alveolar/craniofacial bone regeneration.

Keywords

biomimetic scaffolds; osteogenic; antimicrobial; local delivery; silver nanoparticle; electrospinning

1. INTRODUCTION

Oral and craniofacial tissues are challenging environments for regenerative medicine. The oral cavity is a reservoir for bacterial pathogens and many structures in the craniofacial region are encased or supported by mineralized tissues. As a result, there is a unique need for multifunctional scaffolds with antimicrobial and osteogenic properties for craniofacial tissue engineering. Guided tissue regeneration (GTR) and bone regeneration (GBR) have been important regenerative approaches to restore the health and function of periodontal tissues and craniofacial bone defects. Most commonly, the GTR/GBR membrane is placed into the bone defect area as a barrier to create and maintain a space against the invasion of epithelial and other soft tissues and allow for osteogenic cells to repopulate the osseous defect.[1] Among available GTR/GBR membranes, biodegradable synthetic scaffolds are most attractive because of their biodegradability and capability to serve as a local delivery system to achieve a high local concentration of cargo compounds.[2] Specifically, polymer-based electrospun scaffolds have been continuously improved to incorporate tailored drug-release systems and to ensure cellular integrity while regulating the dynamics of the extracellular microenvironment.[3–5] Due to their biological compatibility and degradability, their flexible mechanical capacity and their controllable bioactive-materials delivery potential,[6] synthetic polymers such as poly-lactic-co-glycolic acid (PLGA), polycaprolactone (PCL) or blends have widely been used for electrospinning into a basic matrix with a 3D porous structure that mimics the arrangement of native extracellular matrix (ECM). This electrospun polymer matrix provides a proper 3D interfiber space sufficient to accommodate for cell adhesion and expansion along randomly-oriented nanofibers.[7] However, osteogenic and antibacterial properties of these synthetic scaffolds are often limited or lacking.

To address the need for multi-layer, complex scaffold materials, mussel-inspired polydopamine coatings have been developed as a straight-forward and effective multifunctional and multipurpose surface modification, replacing physical absorption,

chemical modification, grafting, plasma treatment and other traditional surface modification techniques.[8] The catechol moiety of dopamine, a key component of the mussel adhesive protein, interacts strongly with various materials and forms multifunctional organic/inorganic composite layers consisting of proteins, metal ions, apatites and nanoparticles.[9–11] Several antimicrobial agents have been successfully delivered to equip these synthetic co-polymer scaffolds with effective antimicrobial properties.[12–13]

Current available GTR/GBR membranes are designed to act as a barrier to block connective and epithelial tissue invasion at the periodontal and craniofacial defect sites. To improve their capacity for tissue regeneration, combinations of these membranes with other materials have been explored. For example, silver (Ag)-containing dental materials have been generated for anti-microbial and anti-caries application in oral cavity [14–15]. Silver features a broad-spectrum antimicrobial activity against various bacteria including antibiotic-resistant bacteria, and has been widely used as an anti-infection substance within the medical device field because of its low toxicity to mammalian cells. [16–17] Silver nanoparticles (AgNPs) are characterized by high surface area and unique chemical and physical properties, and may serve as a reservoir for silver ions. As a result, the incorporation and immobilization of AgNPs onto various scaffold fibers using silver ion *in situ* reduction has received much attention.[9, 18] Studies have demonstrated that the effect of AgNPs on cell viability was highly time and dose dependent.[19] Recently, AgNPs have been incorporated into silk fibers using *in situ* approaches, resulting in excellent and long-lasting antibacterial activities against *E. coli* and *S. aureus.* [20] However, these materials remain at the stage of preclinical studies. In contrast, collagen membranes are currently used in medical and dental clinics. Collagen membranes promote wound healing through hemostasis, and provide collagenous scaffold for stem cell homing and tissue regeneration.[21–22] In addition, the effects of collagens on cellular functions including cell attachment, proliferation and differentiation and the effects of biomaterials surface modifications of electrospun polymer scaffolds have been extensively studied.[23–25] However, successful tissue regeneration in the oral cavity and the craniofacial defect microenvironment requires periodontal pathogen control and restauration of the regenerative capacity of mineralized tissues. Therefore, new materials with osteogenic and antibacterial properties are needed for oral and craniofacial tissue regeneration.

In the present study, we have introduced a novel silver-modified/collagen-coated electrospun PLGA/PCL scaffolds (PP-pDA-Ag-COL) as a new biomimetic material with sustained antibacterial and osteogenic properties. For our studies, the biodegradable PLGA/PCL electrospun scaffold was employed as a local delivery system and tailored to feature effective antimicrobial properties with limited antibiotic resistance and to favorably improve osteogenic regeneration. AgNPs *in situ* reduction technology was exploited to coat our PLGA/PCL scaffold via mussel-inspired pDA-coating technology to achieve antibacterial and osteogenic properties and to maintain the three-dimensional interfiber architecture of the scaffold. Type I collagen was then immobilized onto the AgNPs-modified scaffold to improve its osteogenic properties. A schematic illustration of the preparation procedure of scaffolds with their modification is presented in Figure 1. We hypothesized that the incorporation of AgNPs and collagen I into our novel PP-pDA-Ag-COL electrospun scaffolds would lead to good biocompatibility, sustained antibacterial effects and enhanced

osteogenic properties. To characterize the material properties of our novel PP-pDA-Ag-COL scaffold and to assess its potential for guided bone regeneration, we performed physico-mechanical analyses, examined its biocompatibility, and verified its osteogenic and antibacterial potential *in vitro* and *in vivo* in a mouse periodontitis model.

2. EXPERIMENTAL SECTION

2.1 Synthesis of the PP-pDA-Ag-COL Electrospun Scaffolds

PLGA/PCL electrospun scaffolds (PP) were prepared as described previously. [4] To generate a polydopamine coated PLGA/PCL scaffold (PP-pDA), the PP scaffold was immersed into 10mM dopamine hydrochloride (AR, Sigma, USA) solution for 4 h and dry at 40°C for 24 h. AgNPs were then in situ reduced onto the scaffold fibers (PP-pDA-Ag) by immersing the PP scaffold in 10^{-4} M $AgNO_3$ (AR, Sigma, USA) and 10mM dopamine solution for 4 hours. Finally, the PP-pDA-Ag-COL scaffold was generated by coating the PP-pDA-Ag scaffold with 2% collagen I (w/v, rat tail collagen, Waltham, MA, USA) solution. Three intermediate scaffolds, PLGA/PCL (PP), PLGA/PCL-polydopamine (PP-pDA), PLGA/PCL-polydopamine-Ag (PP-pDA-Ag) served as controls.

2.2 Physicochemical Property Testing

2.2.1 Structure and surface characterization—The Surface topography of the PP-pDA-Ag-COL and control scaffolds was characterized using a Field Emission Scanning Electron Microscope (FE-SEM; JSM-7401F, JEOL Ltd., Japan), and diameters of the scaffold fibers were calculated. Following the coating of the samples with AgNPs and collagen I, elemental composition of the scaffold surface was tested by Energy Dispersive X-ray spectroscopy (EDS, Ultra Plus, Zeiss). Surface functional groups were measured by Attenuated Total Reflectance Infrared Spectroscopy (ATR-FTIR) spectra and the contact angles of the samples were investigated using a contact angle meter (SL200B, Solon Technology Science, Shanghai, China) as described previously. [4]

2.2.2 Mechanical property—Rectangular-shaped (10 mm*20 mm*0.16 mm) samples were tested for tensile strength and elastic modulus using the electronic universal testing machine (INSTRON 3365, USA) as stated previously. [4]

2.3 Silver release

The PP-pDA-Ag and PP-pDA-Ag-COL scaffolds with an average weight of 0.021g were immersed in 5 mL of phosphate buffered saline (PBS) at 37℃ for 1, 2, 4, 6, 8, 10, 12, 14, 16, 18, 20 and 21 days. The solution was refreshed and collected every day. The concentration of Ag ion in PBS was analyzed by Inductively Coupled Plasma Mass Spectrometry (ICP-MS, Thermo ICP-MS iCAPQ, ThermoFisher, USA).

2.4 *In vitro* cellular functions

2.4.1 Cell culture—The MC3T3-E1(MC) cell line subclone 14 (Cell Bank of the Chinese Science Academy, Shanghai, China) was cultured and maintained as described previously. [4]

2.4.2 Cell Proliferation—MC cells (2×10^4) were seeded onto 6mm-diameter scaffolds (mean thickness 0.16mm) and cultured in 96-well plates in triplicate for 1, 3, 5 and 7 days. Cell viability and proliferation was tested using Cell Counting Kit-8 (CCK-8; Beyotime, China) according to manufacturer's instruction. An enzyme-linked immunosorbent assay plate reader (Titertek, Helsinki, Finland) was applied to determine the optical density (OD) of formazan at 450 nm in the cell-scaffold groups and scaffold-free cell control.

Cell live/dead staining was performed to investigate the cytotoxicity of the scaffolds using Calcein-AM/PI Double Stain kit (YESEN, Shanghai, China). In brief, MC3T3 cell was cultured for 3 days on the four scaffolds, and collected by centrifugation at 1000 rpm for 5min. The cells were stained with 2 μM calcein-AM (live cells, green fluorescence) and 4.5 μM PI (dead cells, red fluorescence) for 15 min at 37 °C away from light. Images were captured by Inverted fluorescence microscope (Olympus, IX73).

2.4.3 Cell morphology and cell adhesion—Cells (10^4) were seeded onto the 10 mm scaffolds (average thickness of 0.16 mm) and cultured in 24-well plates in triplicate. Surface topography and cell morphology was captured by FESEM and Confocal Laser Scanning Microscopy (CLSM; Zeiss-LSM710; Carl Zeiss, Inc., Jena, Germany) after 24 h and 48 h of the culture. For analysis of cytoskeleton, samples were fixed and stained with rhodamine phalloidin (Cytoskeleton, Inc., Denver, CO, USA).

2.5 Integrin β1 Immun of luorescence

After 24 hours culture, samples were prepared as described previously. In brief, cells were incubated with anti-integrin β1 antibody (Abcam, ab52971) overnight followed with the incubation of secondary anti-rabbit IgG antibody (Alexa Fluor 488 goat, Beyotime, Shanghai, China) and rhodamine phalloidin for 15 min at room temperature. Images were captured using a Zeiss LSM 710 microscope and analyzed by the CLSM image browser.

2.6 RNA Isolation and RT-PCR

Total RNAs were extracted using the TRIzol reagent (Invitrogen). The reverse transcription reactions were performed by the PrimeScript RT reagent kit (Clontech, Mountain View, CA). The SYBR Premix Ex Taq kit (Clontech) was applied for Real-time PCR reactions using cDNA as the template. The sequences of primers used in this study are listed in Table 1. The reaction included initial denaturation at 95 °C for 5 min; 40 cycles at 95 °C for 10 s, 60 °C for 31 s (ABI 7300 Real-time PCR System). The values of target gene expression were normalized to GAPDH and the relative expression levels were calculated by the $2^{-\Delta\Delta Ct}$ method.

2.7 Alkaline Phosphatase (ALP) Assays

MC3T3 cells were collected by subjecting the scaffolds to centrifugation at 1000 rpm for 5 min. The cells were lysed with RIPA buffer. Cell lysates were homogenized and centrifuged to remove insoluble material at full speed for 3 minutes, and the supernatants were collected for ALP testing. The ALP activity was determined using the Alkaline Phosphatase Assay kit (Beyotime), and the OD values were measured via a microplate reader (Multiskan MK3,

Thermo Scientific, Shanghai) at 405nm. ALP activity was normalized to the total protein content.

2.8 Western Blot

Total protein was extracted from collected cells with RIPA buffer. The Bradford method was used to assess the protein concentration. Western blot analysis was performed as described previously.[4] Anti-BMP2 (ab14933), anti-Runx2 (ab23981) and anti-rabbit IgG (ab6721) antibodies were obtained from Abcam. GAPDH (ab8245) was used as an internal control. The results were analyzed by the ImageJ (NIH, Bethesda, USA) and GraphPad Prime 5.0 software.

2.9 Antibacterial Tests

2.9.1 Bacterial inoculation—An agar diffusion test was conducted in independent triplicates with *Staphylococcus aureus* (*S. aureus*) inoculated in LB agar and *Streptococcus mutans* (*S. mutans*) inoculated in Brian Heart Infusion agar, respectively. 6mm-diameter scaffolds were punched and gently placed with sample distance from each other on the surface of the 15 mL nutrient agars containing 1 mL of bacterial suspension in 0.9% NaCl (104 CFU/ml) by the plate pouring method. The diameter of the inhibition zone (DIZ) around the scaffolds after 24h incubation at 37 °C was measured to reflect the antibacterial activity of each scaffold.

2.9.2 Bacterial attachment and bacterial fluorescence on scaffolds—*S. aureus* and *S. mutans* were used to estimate the bacterial attachment on the scaffolds. Scaffolds were cultured with 1 ml bacterial suspension in 48-well plates at 37 °C for 24 h and then dehydrated with a series of ethanol solutions (30, 50, 70, 90, and 100%), and finally evaporated to constant weight at room temperature under vacuum. Surface topography and antibacterial ability of the scaffolds was observed by FESEM. For bacterial fluorescence, each scaffold was incubated with 1 ml bacterial suspension in a 48-well plate for 24 h at 37 °C, washed 3 times with PBS, fixed with 3.7% paraformaldehyde for 30 min, permeabilized with 0.25% Triton X-100/PBS for 5 min, and finally stained with DAPI for 10 min in the dark at room temperature. Bacterial fluorescence was captured by CLSM.

2.10 In vivo evaluation of tissue regeneration effect

2.10.1 Subcutaneous implantation—A total of 5 male C57BL/j mice at age of eight weeks were obtained from Charles River Laboratory (Huston, TX) and bred at Texas A&M Colleg of Dentistry in strick accordance with the recommendations on the Guide for Care and Use of Laboratory Animals of the National Institution of Health. PP-pDA-Ag-COL and three control scaffolds (5mm in diameter) were implanted into the back of these mice below the subcutis. The mice were sacrificed 10 days after implantation and the implants were dissected and prepared for histological examination.

2.10.2 Mouse periodontitis model and GTR treatment—This model relies on eight-week-old male and female C57BL/j mice (Charles River). To induce periodontitis, sutures (5–0 silk sutures) were placed around left maxillary second molars [26]. A total of 20 mice (n=5) were divided into three GTR groups (periodontitis/GTR-PP-pDA-Ag-COL,

periodontitis/GTR-PP-pDA-Ag and periodontitis/GTR-PP) as well as defect control (periodontitis/no GTR). To mimic a clinical situation and to readily access periodontitis-related bone defects, mice were subjected to gingival flap surgery. For flap surgery, incisions were placed from the mesial surface of the first molar to the distal surface of the third molar on the left maxilla. Full-thickness flaps were then elevated and PP-pDA-Ag-COL and control scaffolds were applied to the surface of the exposed alveolar bone. The flaps were then repositioned and sutured in place.

2.10.3 Tissue Processing and histological Staining—Implants or maxillae were dissected, fixed and demineralized. The demineralized samples were embedded in paraffin and then sectioned. For hematoxylin and eosin (H&E) staining, deparaffinized and rehydrated sections were dipped in hematoxylin for 3 min and in eosin for 1 min, then dehydrated in an ascending ethanol series and cleared in xylene. For Mallory's Trichrome staining, sections were stained using Mallory's Trichrome staining kit (American MaterTech Sicentific, St Lodi, CA) according to the manufacturer's instructions.

2.10.4 μCT analysis—To evaluate the effect of scaffolds on new bone formation and bone remodeling, μCT images from left maxillae after 6-week GTR were captured and bone volume and mineral density were analyzed using a Scanco 40 μCT apparatus (Scanco Medical, Wayne, PA). Alveolar bone loss was calculated as the area (mm^2) bordered by the cemento-enamel junction, the crest of alveolar bone, and the mesial and distal line angles on the buccal and lingual sides of maxillary molars[26].(Figure S1) The samples were then processed for paraffin section and staining.

2.11 Statistical Analysis.

SPSS ver22 (SPSS, Chicago, IL, U.S.A.) was used for data analyses. All experimental data were shown as mean ± standard deviation (Mean ± SD). One-way analysis of variance and the least significant difference test were performed at $p = 0.05$ after the normality was tested. All quantitative data were represented by the mean of at least three independent experiments.

3. RESULTS AND DISCUSSION

3.1 Surface topography of the PP-pDA-Ag-COL and control scaffolds

SEM analysis demonstrated that all four electrospun scaffolds featured highly-interconnected porosity and randomly-oriented filamentous 3D architecture with clearly distinguished inter-fiber spaces (Figures. 2Aa–Dd). The average nanofiber diameter in the PP scaffold was 427±149 nm. This scaffold consisted of a smooth surface with high interconnected porosity. The nanofiber diameter in the PP-pDA scaffold was 484±263 nm, and the fiber surfaces were relatively rough following pDA coating. PP-pDA-Ag and PP-pDA-Ag-COL scaffold contained nanofibers with a diameter of 492±207 nm and 477±186 nm, respectively. The elemental composition of the scaffolds was determined by EDS (Figure 2As–Ds, E). In comparison with PP-pDA-Ag, the silver atomic ratio of PP-pDA-Ag-COL decreased from 0.11% to 0.02% while the C/O ratio increased slightly, signifying the successful immobilization of collagen I onto the PP-pDA-Ag surface. However, nitrogen

content in these scaffolds was below detection threshold, indicating a low collagen content originating from the scaffold coating.

Electrospinning produces nanofibrous scaffolds with an assembly pattern similar to the native extracellular matrix (ECM) including 3D inter-fiber spaces that will accommodate cells. Surface modifications enhance the functionalities of electrospun scaffolds while largely maintaining the original 3D scaffolding framework[27]. In the present study, we generated an original PP scaffold as a baseline control and then modified the PP scaffolds with pDA only, pDA plus AgNPs or pDA plus AgNPs and type I Collagen. These modifications slightly increased the diameter and roughness of the scaffold fibers (Figure 2). However, the modified scaffolds maintained the randomly orientated fibrous structure mimicking ECM architecture. In addition, all four electrospun scaffolds featured a pore size and porosity that enables adequate flow of nutrients and oxygen and is essential for successful hard-tissue regeneration[27]. When these sacffolds were subjected to the degradation test[28] up to 4 weeks, the mass drop-off of PP, PP-pDA, PP-pDA-Ag and PP-pDA-Ag-COL was 3.5%, 7.8%, 15.5% and 8.5% respectively (Figure S2). This result is consistent with the report from Ott and colleagues that co-spun PLGA/PCL scaffolds retained their unique co-spun fiber morphology after 6 weeks of sample degradation, and only regained a normal fibrous morphology at week 12.[28]

3.2 Physicochemical properties of the PP-pDA-Ag-COL and control scaffolds

Infrared spectra of PP, PP-pDA, PP-pDA-Ag and PP-pDA-Ag-COL (Figure 3A) revealed characteristic patterns of PLGA scaffolds, including free-bonded ester group peaks at 1757 and 1727 cm^{-1} attributed to PLGA [29] and the conjugated C=O group in PCL respectively. [30] There were also amide and hydroxyl peaks at 3000 and 3400 cm^{-1} in PP-pDA, indicative of the presence of a pDA layer in PLGA/PCL (PP). [31] The IR spectra did not reveal any significant difference between the functional groups of PP-pDA-Ag and PP-pDA. We assigned the peaks at 1630 and 1552 cm^{-1} in the PP-pDA-Ag-COL spectra as the N-H_2 and N-H amide I groups, respectively. [32] The broad peaks at 3381 cm^{-1} were related to the hydroxyl and amide groups in COL I, suggesting successful coating of COL I onto the scaffolds.

Mechanical strength of the biodegraded nanofibers plays an important role in mimicking natural materials. As shown in Figure 3B, the mean Young's modulus values of the synthetic PP, PP-pDA, PP-pDA-Ag and PP-pDA-Ag-COL were 48.7±16.2, 56.3±25.5, 18.6±3.5 and 30.5±12.6 MPa while the fracture stress values of PP, PP-pDA, PP-pDA-Ag and PP-pDA-Ag-COL were 2.2±0.7, 1.5±0.7, 2.2±1.1 and 1.3±0.1 MPa, respectively. The mechanical properties of the PP-pDA-Ag-COL scaffold were similar with that of the PP scaffold and in the same range as the electrospun PLGA/PCL membranes developed by Chou et al[33]. In contrast, the PP-pDA scaffold had higher elastic modulus but lower fracture stress while the PP-pDA-Ag scaffold had lower elastic modulus but higher fracture stress when compared to the PP scaffold. These results indicate that PP-pDA-Ag-COL maintained the elasticity modulus and fracture stress after surface modification.

The water contact angle was tested to determine the hydrophilic properties of our scaffolds (Figure 3C). The contact angles of PP, PP-pDA, PP-pDA-Ag and PP-pDA-Ag-COL were

126.6±9.2°, 81.7±6.9°, 104.6±5.7° and 30.2±6.2°, respectively. The pDA coating rendered the PP-pDA surface more hydrophilic by decreasing the contact angle.[34] The load of AgNPs on the surface of the scaffolds through pDA coating created a rough surface and increased the water contact angle.[35] However, after type I collagen coating, the contact angle of PP-pDA-Ag-COL dropped significantly to 30.2±6.2° and the hydrophilic properties of the PP-pDA-Ag-COL were improved compared to the three control scaffolds. These results demonstrated that the modification of electrospun PP scaffolds with silver *in situ* reduction by pDA coating and type I collagen incorporation increased its hydrophilic properties and provides a better physiological environment for cell growth .[36]

3.3 Silver ion release from two silver-modified scaffolds

The accumulated release of silver ions from the PP-pDA-Ag and PP-pDA-Ag-COL scaffolds in PBS (pH = 7.4) over a period of 21 days is shown in Figure 4. The cumulative concentration of silver ions controlled-released from the two Ag-modified scaffolds gradually increased over 16 days and was steady thereafter from day 16 to day 21. The release rate of PP-pDA-Ag-COL was slower than that of PP-pDA-Ag, which is probably due to the coverage of COL I on the surface of the scaffold. The release of silver ions depends on the oxidation of AgNPs and the hydrolysis of silver oxide (AgO). The collagen layer effectively prevented the direct contact between the AgNPs with air-saturated aqueous solutions, so that only limited amounts of oxygen (O2) and hydrogen ions (H+) reacted with the AgNPs, resulting in a slower Ag^+ release rate.[37] The accumulated silver ion concentration was about 0.05535μg/ml (0.513 μmol/l) at day 14 and 0.0581μg/ml (0.539 μmol/l) at day 21, which is in the range of non-cytotoxic and effective antibacterial effects (0.25-1μmol/l or 2.5×10^{-7}M- 10^{-6}M) .[38] This result supports the applicability of PLGA/PCL electrospun scaffolds as local-delivery systems releasing silver ions steadily and effectively to the target area without toxicity to living tissues.

3.4 The effects of the scaffolds on MC3T3 cellular functions

3.4.1 Cell proliferation—MC3TC cells were cultured with four scaffolds to investigate the effect of our scaffolds on the cell proliferation. Cell proliferative capability was evaluated based on CCK-8 assays. To determine an optimal silver ion concentration for impregnation of the PP-pDA-Ag scaffold, PP-pDA scaffolds were immersed in $AgNO_3$ solution with different concentrations of 1×10^{-3}M, 5×10^{-4}M, 1×10^{-4}M and 5×10^{-5}M. As illustrated in Figure 5A, MC3T3 cells cultured on PP-pDA-Ag generated from a 1×10^{-4}M $AgNO_3$ solution had the highest cell viability and proliferation rate at 1, 3, 5 and 7 days of culture when compared to controls. Therefore, 1×10^{-4}M $AgNO_3$ solution was applied in subsequent studies. As shown in Figure 5B, MC3T3 cells cultured on PP-pDA-Ag (1×10^{-4}M) and PP-pDA-Ag-COL (1×10^{-4}M) were associated with increasing proliferation rates after 1, 3, 5 and 7 days of the culture, and the PP-pDA-Ag-COL scaffold was associated with the highest proliferation rates (Figure 5B), suggesting that PP-pDA-Ag-COL enhanced cell proliferation after immobilization of a proper amount of AgNPs and COL I.

The proliferation rate of MC3T3 cells cultured on the two silver-modified scaffolds was significantly higher at day 1 and day 3, probably due to the low concentration of Ag^+ controlled-release. Although previous studies have documented that the effects of AgNPs are

time-dependent and dose-dependent on cytotoxicity and cell proliferation,[19] low concentrations of Ag^+ are capable of promoting MC cell proliferation.[39] MC3T3 cells cultured on the PP-pDA-Ag-COL scaffold exhibited the greatest increase in proliferation at all time-points tested in the present study. This result was confirmed by the live/dead calcein staining of MC3T3 cells using the Live-Dead Cytotoxicity Kit (Figure 6). There were 268±19/field (PP-pDA-Ag-COL), 156±14/field (PP-pDA-Ag), 92±2/field (PP-pDA) and 85±6/field (PP) cells were stained with green fluorescence while only 15±1/field (PP-pDA-Ag-COL), 27±2/field (PP-pDA-Ag), 19±2/field (PP-pDA) and 12±1/field (PP) cells were stained in red fluorescence in each field, indicating their good cytocompatibility. The data from our studies further confirm that immobilization of ECM proteins such as type I collagen, [40] and fibronectin[41] facilitates the interaction between the cells and material surfaces by modulating cell adhesion and proliferation. In addition, changes in surface topography and chemistry by collagen coating are known to affect cell proliferation as well (Figure 5B) [42].

3.4.2 Cell morphology and attachment—We used a FESEM to understand how our PP-pDA-Ag-COL and control scaffolds affected the interaction between MC3T3 cells and their environment, including cell morphology, cell attachment and spreading. Figure 7A illustrated that cells spread along the randomly-oriented nanofibers and extended filopodia in the same directions as the nanofiber orientations. The 3D-porous structure of all four scaffolds provided suitable microenvironments to accommodate MC3T3 cells, indicative of the well-designed structure of these 3D electrospun scaffolds for cell inhabitation and their ability to create a favorable microenvironment for cell recruitment. There were more cells attached on the PP-pDA-Ag-COL scaffold when compared to the other scaffolds. In opposite to cells on control scaffolds, cells on the PP-pDA-Ag-COL scaffold displayed elongated shapes and were detected in the interfiber spaces (Figure 7A), suggesting that PP-pDA-Ag-COL enhanced MC3T3 cells attachment and spreading.

The effect of our scaffold surfaces on MC3T3 cell cytoskeletal morphology after 12h and 24h culture was revealed using fluorescence microscopy (Figure 7B). Confocal micrographs provided evidence for the 3D distribution of MC3T3 cells, cell attachment and scaffold infiltration for all four electrospun scaffolds. Confocal images demonstrated that the cells have exquisite actin fibers and filopodia extended three-dimensionally along the invisible randomly-oriented nanofibers in multiple directions. After 12 hours, MC3T3 cells cultured on the PP-pDA and PP-pDA-Ag scaffolds spread slightly better than on the PP scaffold, and MC3T3 cells exhibited the widest range of spreading on our PP-pDA-Ag-COL scaffold. After 24h culture, cell spreading was improved on all scaffolds compared to cell spreading after 12 h culture (Figure 7B). After 12h and 24h culture, the actin cytoskeleton of MC3T3 cells attached to the PP-pDA-Ag-COL scaffold spread and stretched further than cells on the other three scaffolds. This finding is consistent with our SEM results, further confirming that PP-pDA-Ag-COL scaffolds promoted cell attachment and spreading.

3.4.3 The effects of the scaffolds on integrin expression in MC3T3 cells—The interaction between cells and microenvironment, either from the ECM or from implanted biomaterials is modulated by integrin cell surface receptors.[43] Integrins are composed of an

α chain and a β chain, and interact with the extracellular matrix through the RGD domain or the DGEA (Asp-Gly-Glu-Ala) sequence of ECM proteins. In this study, MC3T3 cells were cultured on the PP-pDA-Ag-COL and control scaffolds for 12, 24 and 48 hours, and the expression of α1, α2, α5, α10, α11 and β1 integrin was analyzed using real time RT-PCR analysis (Figure 8). After 12 hours of culture, the expression of all six integrins was significantly upregulated in the PP-pDA, PP-pDA-Ag and PP-pDA-Ag-COL groups compared to the PP group ($p < 0.05$). The expression levels of integrin α1, α2, α10, α11 and β1 were generally higher than that of α5 at three time points, except for the expression of integrin α2 after 24 hours. Supporting our materials design approach, the PP-pDA-Ag-COL scaffold promoted consistently higher integrin α11 and β1 expression levels after 12, 24 and 48 hours culture (Figure 8), indicative of the impact of collagen incorporation into the scaffold on integrin expression in MC3T3 cells.

Upregulation of integrin β1 expression at the protein level in MC3T3 cells cultured on PP-pDA, PP-pDA-Ag and PP-pDA-Ag-COL scaffolds was further confirmed using immunofluorescence (Figure 9). Confocal microscopy images demonstrated all three dopamine modified scaffolds enhanced integrin β1 expression. Especially, PP-pDA-Ag-COL promoted highest β1 integrin expression levels in MC3T3 cells after 24h culture on the scaffold when compared to the control scaffolds (Figure 9).

Integrins α1, α2, α5, α10, α11 and β1 participate in cell adhesion and cell-surface mediated signaling. Integrins α1, α2, α10 and α11 dimerize with β1 integrin individually to form collagen receptors α1β1, α2β1, α10β1 and α11β1, while integrin α5 joins β1 integrin to form the fibronectin receptor α5β1.[44] Previous studies have confirmed that polydopamine promotes cell adherence, proliferation, and differentiation of osteoblasts on pDA-coated substrates[45–46] and that dopamine activates integrin function through its receptors.[42] Here we first demonstrated that polydopamine coating on the scaffold surface increased the expression of collagen receptors α1β1, α2β1, α10β1 and α11β1 and of fibronectin receptor α5β1. The upregulation of α1, α2, α10 and α11 expression was more pronounced than that of α5, indicating that pDA-coated PP scaffolds promoted the interactions between MC3T3 cells and collagens. Second, incorporation of type 1 collagen into polydopamine-coated scaffold resulted in further higher expression of α1, α2, α10, α11 and β1 integrins almost at all three time points. These findings may be explained by the preferred binding activity of type I collagen to the collagen receptor α11β1, [47–48] and affecting other collagen receptor activities. Third, the effect of polydopamine on integrin expression was slightly reduced by the incorporation of Ag into the scaffolds after 24 hours' cell culture, indicating that binding of Ag to polydopamine may affect the bio-adhesive function of polydopamine. However, the influence of Ag on polydopamine function was decreased after release of Ag from the scaffolds after 48h culture. The gene expression of α1, α2, α10, α11 and β1 in the PP-pDA-Ag group were again up-regulated ($p < 0.01$). Only the expression of integrin α5 in the PP-pDA-Ag group was lower than that in PP-pDA group after 48h culture, indicating that the interaction between silver and pDA-coating can lead to less expression of integrin α5, although Cao et al. reported that AgNPs immobilized on titanium could motivate integrin α5 and augment cell adhesion.[49]

3.4.4 Cell differentiation—Alkaline phosphatase (ALP) activity is one of the markers for early osteoblastic differentiation and mineralization.[50] Here we have tested the ALP activity of MC3T3 cells cultured on our four scaffolds. Our data revealed that the ALP activity of MC3T3 cells cultured on PP-pDA, PP-pDA-Ag and PP-pDA-Ag-COL increased over time and was higher when compared to MC3T3 cells cultured on the PP scaffold ($p < 0.05$) (Figure 10A and B), indicating that the functionalized scaffolds accelerated osteogenic differentiation of MC3T3 cells. In addition, PP-pDA-Ag-COL significantly enhanced MC3T3 cell differentiation 7 or 14days after induction when compare with the other three scaffolds.

The osteogenic differentiation of mesenchymal stem cells is regulated by growth factors such as BMP2 and transcription factors such as RUNX2. [51–52] In this study, Western blot analysis revealed that BMP2 and RUNX2 expression levels were significantly upregulated in MC3T3 cultured on PP-pDA, PP-pDA-Ag and PP-pDA-Ag-COL at day 7 and day 14, when compared to PP as shown in Figure 10C–F. The effect on BMP2 and RUNX2 expression levels was in the order of PP< PP-pDA< PP-pDA-Ag< PP-pDA-Ag-COL ($p < 0.05$), suggesting that surface modifications on PLGA/PCL scaffold by pDA assisted AgNPs and collagen I incorporation enhanced MC3T3 cell differentiation. PP-pDA-Ag-COL displayed the highest expression levels of BMP2 and RUNX2, probably owing to the synergistic effects of immobilizing AgNPs and collagen I onto PLGA/PCL electrospun scaffolds by pDA-coating.

Previous studies have indicated that different sizes and concentrations of AgNPs may have distinct effects on stem cell differentiation[53]. Specifically, AgNPs increase the reactive surface area and simultaneously release silver ions at low concentrations. When human mesenchymal stem cells were cultured with AgNPs under osteogenic lineage induction conditions, low concentrations of AgNPs (≤ 0.25μg/ml final Ag^+ concentration) increased osteogenic differentiation without toxicity to cells.[54] AgNPs also accelerated proliferation and differentiation, and significantly enhanced the differentiation and mineralization of MC3T3 cells .[49, 55] In our study, the steady silver ion release rate of PP-pDA-Ag-COL within 21days was 0.0581μg/ml, which appeared to significantly promote MC3T3 cell differentiation. AgNPs were also found to stimulate osteogenesis by activating the integrin α5 orchestrated MAPK/ERK signal cascade in rat bone marrow stem cells. [56] This finding is consistent with the upregulation of integrin α5 expression in MC3T3 cells cultured on the polydopamine modified PP-pDa, PP-pDA-Ag and PP-pDA-Ag-COL scaffolds in this study. In addition to the upregulation of integrin α5 expression, these scaffolds significantly increased the expression of collagen receptors in MC3T3 cells (Figure 9 and 10). Scaffold coating with the principal ECM protein collagen facilitated MSC differentiation into mesenchymal cell lineages including osteoblasts, chondrocytes, and cardiomyocytes [57–61] Here we have demonstrated that the PP-pDA-Ag-COL scaffold enhanced ALP activity and increased BMP2 and RUNX2 expression. BMP2 potently induces osteoblast differentiation[62] and RUNX2 is a key transcription factor associated with osteoblast differentiation and controls osteoblast phenotype differentiation and functions.[63] Both BMP2 and RUNX2 are bone specific markers and used in this study to assess the level of osteogenic differentiation of MC3T3 cells cultured on the scaffolds. Our results

demonstrated that immobilized AgNPs and collagen coating by polydopamine promoted MC3T3 cell adhesion, proliferation and osteogenic differentiation, matching earlier studies.[64]

3.5 Antibacterial properties

Prevention of infection is an important attribute for the clinical application of scaffolds in the complex environment of the oral cavity because of the high concentration of bacteria in saliva and on the mucosal surfaces. In the present study we impregnated our PLGA/PCL scaffold with AgNPs to improve its antimicrobial properties for potential clinical applications. In Figures 11A and B, two AgNPs-modified scaffolds PP-pDA-Ag and PP-pDA-Ag-COL displayed a significantly wider antibacterial zone than the control PP-pDA after 24h inoculation against *S. aureus* and *S. mutans* (Table S1). PP-pDA-Ag exhibited 13.52±0.1mm DIZ against *S. aureus* and 9.06±0.3mm DIZ against *S. mutans* while PP-pDA-Ag-COL displayed 12.51±0.1mm DIZ against *S. aureus* and 7.52±0.1mm DIZ against *S. mutans,* suggesting that the antibacterial ability of PP-pDA-Ag was slightly stronger than that of PP-pDA-Ag-COL. While less effective in terms of immediate Ag^+ release, we anticipate that the COL I layer will contribute to the long-term controlled-release of Ag^+. The PP-pDA-Ag and PP-pDA-Ag-COL scaffolds inhibited bacterial growth after 24h incubation with *S. aureus* and *S. mutans* and the morphology and distribution of the bacteria on the scaffolds was analyzed by SEM and CLSM. As demonstrated in Figure 11C and D, *S. aureus* and *S. mutans* were distributed at high density on the PP and PP-pDA scaffolds in SEM images while there were relatively few bacteria on the PP-pDA-Ag and PP-pDA-Ag-COL scaffolds. These results are consistent with the CLSM images (Figure 11E and F). There were much less bacteria stained by DAPI on the PP-pDA-Ag and PP-pDA-Ag-COL scaffolds than on the PP and PP-pDA scaffolds. Summarizing the result from the microbiological studies, PP-pDA-Ag and PP-pDA-Ag-COL significantly inhibited *S. mutans* and *S. aureus* through the controlled release of silver ions from AgNPs.

Silver nanoparticles have broad antibacterial, antiviral, and antifungal properties with a very low potential to induce antibacterial resistance.[65] The antimicrobial properties of silver nanoparticles depend on the release of biologically active silver ions (Ag^+). The oxidative state of silver is vital to the antibacterial effect of silver. When silver is exposed to aqueous media, the adsorbed atomic oxygen on the surface of silver reacts with pairs of sulfhydryl (-S-H) groups on the surface of bacteria or viruses and replaces the hydrogen atoms. As a result, the sulfur atoms form an R-S-S-R bond, which completely blocks respiration and electron transfer. The resulting stable –S-Ag group inhibits hydrogen transfer.[66] Moreover, the reactive oxygen species (ROS) produced by Ag^+ invade the bacteria through ion channels, which results in oxidative membrane damage and eventually bacterial cell death.[67–68]

Previously it has been assumed that silver is more toxic toward prokaryotic cells than toward mammalian cells. However, recent studies have argued that silver ions and nanoparticles in bacteria and human cells have a similar toxic effect with concentrations ranging from 0.5 to 5 ppm for silver ions and 12.5 to 50 ppm for silver nanoparticles.[69–70] In the present study, we generated AgNPs modified scaffolds prepared with $AgNO_3$ at a concentration of 10^{-4} M.

Controlled-release analysis of silver ions revealed that the accumulated concentration of Ag^+ ions at day 14 and day 21 was 0.055 and 0.058 g/ml, respectively. Our data indicated that this relatively low Ag ion release rate was sufficient to effectively inhibit bacteria growth. In addition, MC3T3 cell viability and proliferation was increased and these cells underwent osteogenic differentiation after incubation with these scaffolds. Our studies demonstrated that Ag^+ ions at these concentrations exerted significant effect on the inhibition of bacterial growth, and also promoted MC3T3 cell proliferation and differentiation.

3.6 *In vivo* effect on stem cell recruitment and periodontal regeneration

3.6.1 Subcutaneous implantation—To determine the in vivo application of PP-pDA-Ag-COL and control scaffolds for stem cell recruitment and growth, the scaffolds were implanted subcutaneously. Cell numbers penetrated into four scaffolds were 117±16/field (PP-pDA-Ag-COL), 67±3/field (PP-pDA-Ag), 38±19/field (PP-pDA) and 34±15/field (PP), respectively. PP-pDA-Ag-COL had significantly more cell infiltration than three control scaffolds, suggesting that PP-pDA-Ag-COL had optimal biocompatibility and biomimetic capacity to accommodate cell recruitment. However, no differences were found in term of the number of cell infiltration and collagen matrix formation between PP and PP-pDA (Figure 12), implying that PP and PP-pDA had similar cell response. Furthermore, less elastic fibers and more collagen matrix existed in PP-pDA-Ag-COL scaffold (Figure 12). This result instructed us to use only PP as GTR control scaffold for the further periodontal tissue regeneration in the mouse periodontitis model.

3.6.2 Periodontal tissue regeneration in a mouse periodontitis model—To determine whether our novel PP-pDA-Ag-COL displayed any effects on microbial growth and/or bone regeneration, scaffolds and controls were implanted as GTR membranes into the alveolar bone defects of mice suffering periodontitis for up to 6 weeks. 3D reconstruction of μCT images demonstrated that the distances between alveolar bone ridges and the cementum-enamel junction (CE junction) of maxillary molars were significantly decreased (Figure 13A) in the PP-pDA-Ag-COL group. Alveolar bone loss was reduced by 31.8% in the PP-pDA-Ag-COL group, 24.9% in the PP-pDA-Ag group and 15.1% in the PP group when compared to the periodontitis control group (Figure 13C), indicating that the PP membranes facilitated periodontal tissue regeneration similar to known GTR membranes, and this effect was enhanced by the Ag/COL modifications. The bone volume in PP-pDA-Ag-COL was significantly enhanced compared to the periodontitis control, PP and PP-pDA-Ag (Figure 13D). However, no significant difference was found in bone mineral density of the alveolar bone in periodontitis control, PP, PP-pDA-Ag and PP-pDA-Ag-COL (Figure 13E).

Guided tissue regeneration of periodontal defects involves infection control as well as restoration of alveolar bone loss. It is will-known that the GTR sites are susceptible to periodontal bacteria and plaque control is a critical stem in periodontal therapy.[71–72] Meanwhile, recruitment of desired stem cells to repopulate defect sites and regenerate lost alveolar bone are equally important for periodontal GTR. In the present study, we generated a novel scaffold with both antimicrobial and osteogenic properties. The PP-pDA-Ag-COL scaffolds meet the criteria for GTR/GBR procedures. We have demonstrated that the PP-

pDA-Ag-COL inhibited bacterial growth (Figure 11), provided a microenvironment for stem cell recruitment and collagen matrix formation (Figure 12), reduced the distance between the cemento-enamel junction and the recessed alveolar bone ridge, and enhanced alveolar bone regeneration. Our study confirms that our PP-pDA-Ag-COL scaffolds facilitate periodontal tissue regeneration thought antibacterial effects and osteogenic stimuli in the periodontal defects.

In summary, the mechanical and chemical properties of 3D electrospun nanofibrous scaffolds can be tailored to improve the osteogenic differentiation of stem cells and craniofacial bone formation including periodontal tissue regeneration[73]. In the present study, Ag ions were controlled-released from PP-pDA-Ag and PP-pDA-Ag-COL scaffolds and exhibited inhibitory functions in infection and inflammation (Figure 11). In addition, incorporation of collagen into PP membranes enhanced cell attachment and osteogenic differentiation of MC3T3 cells (Figure 7–10). Furthermore, our *in vivo* results suggested that the AgNPs/COL-modified 3D scaffolds provide desired microenvironments for periodontal tissue regeneration.

4. Conclusion

In the present study, structural materials design and surface modification technologies were combined to engineer a novel scaffold with effective antimicrobial and improved osteogenic properties. AgNPs were modified to impregnate PLGA/PCL electrospun scaffolds via silver ion *in-situ* reduction using a mussel-inspired pDA coating technology, which then resulted in the steady release of silver ions even after collagen I coating. As a result, our PLGA/PCL electrospun scaffolds became a functional matrix that prevented infection and enhanced bone mineralization by incorporating AgNPs and collagen I. The benefits of our novel PP-pDA-Ag-COL I scaffold include reduction of antibiotic load with limited antibiotic resistance and improvement of bone regeneration. In conclusion, our novel silver-modified/collagen-coated electrospun PLGA/PCL scaffold features biocompatible, osteogenic and antibacterial properties indicative of its therapeutic potential for craniofacial bone regeneration.

Supplementary Material

Refer to Web version on PubMed Central for supplementary material.

ACKNOWLEDGMENT

This work was supported by the National Natural Science Foundation of China [81801025 (Y. Q.), 31200757 (X.Z.)], the National Key Research and Development Plan (2016YFA0201704) (F.Z.), the Suzhou Health and Family Planning Commission (SYSD2015093) (Y.Q.), Suzhou science and technology development project (SYG201719) (X.Z.), the Preponderant Clinic Discipline Group Project Funding of the Second Affiliated Hospital of Soochow University (No. XKQ2015010) (J.Y. and Y.Q.), the Advanced Research Program of the Second Affiliated Hospital of Soochow University (SDFEYBS1603) (Y.Q.). Additional funding was provided by the following grants from the National Institute of Dental and Craniofacial Research: 2R01DE019463-03A1 (X.L.), R01 DE027930 and R01 DE DE026198 (T.G.H.D.).

REFERENCES

(1). Bottino MC; Thomas V; Schmidt G; Vohra YK; Chu TMG; Kowolik MJ; Janowski GM Recent advances in the development of GTR/GBR membranes for periodontal regeneration-A materials perspective. Dent. Mater. 2012, *28* (7), 703–721, DOI: 10.1016/j.dental.2012.04.022. [PubMed: 22592164]

(2). Soldatos NK; Stylianou P; Koidou VP; Angelov N; Yukna R; Romanos GE Limitations and options using resorbable versus nonresorbable membranes for successful guided bone regeneration. Quintessence Int. 2017, 48 (2), 131–147. [PubMed: 27834419]

(3). Huang GY; Li F; Zhao X; Ma YF; Li YH; Lin M; Jin GR; Lu TJ; Genin GM; Xu F Functional and Biomimetic Materials for Engineering of the Three-Dimensional Cell Microenvironment. Chem. Rev. 2017, 117 (20), 12764–12850, DOI: 10.1021/acs.chemrev.7b00094. [PubMed: 28991456]

(4). Qian YZ; Zhou XF; Sun H; Yang JX; Chen Y; Li C; Wang HJ; Xing T; Zhang FM; Gu N Biomimetic Domain-Active Electrospun Scaffolds Facilitating Bone Regeneration Synergistically with Antibacterial Efficacy for Bone Defects. ACS Appl. Mater. Interfaces 2018, 10 (4), 3248–3259, DOI: 10.1021/acsami.7b14524. [PubMed: 29172421]

(5). Wang JL; Wang LN; Zhou ZY; Lai HJ; Xu P; Liao L; Wei JC Biodegradable Polymer Membranes Applied in Guided Bone/Tissue Regeneration: A Review. Polymers 2016, 8 (4), 20, DOI: 10.3390/polym8040115.

(6). Martin V; Bettencourt A Bone regeneration: Biomaterials as local delivery systems with improved osteoinductive properties. Mater. Sci. Eng. C-Mater. Biol. Appl. 2018, 82, 363–371, DOI: 10.1016/j.msec.2017.04.038. [PubMed: 29025670]

(7). Qian YZ; Chen HB; Xu Y; Yang JX; Zhou XF; Zhang FM; Gu N The preosteoblast response of electrospinning PLGA/PCL nanofibers: effects of biomimetic architecture and collagen I. Int. J. Nanomed. 2016, 11, 4157–4171, DOI: 10.2147/ijn.s110577.

(8). Ryu JH; Messersmith PB; Lee H Polydopamine Surface Chemistry: A Decade of Discovery. ACS Appl. Mater. Interfaces 2018, 10 (9), 7523–7540, DOI: 10.1021/acsami.7b19865. [PubMed: 29465221]

(9). Song YY; Jiang HJ; Wang BB; Kong Y; Chen J Silver-Incorporated Mussel-Inspired Polydopamine Coatings on Mesoporous Silica as an Efficient Nanocatalyst and Antimicrobial Agent. ACS Appl. Mater. Interfaces 2018, 10 (2), 1792–1801, DOI: 10.1021/acsami.7b18136. [PubMed: 29303548]

(10). Pan HT; Zheng QX; Yang SH; Guo XD Effects of functionalization of PLGA- Asp-PEG n copolymer surfaces with Arg-Gly-Asp peptides, hydroxyapatite nanoparticles, and BMP-2-derived peptides on cell behavior in vitro. J. Biomed. Mater. Res. Part A 2014, 102 (12), 4526–4535, DOI: 10.1002/jbm.a.35129.

(11). La WG; Shin JY; Bhang SH; Jin M; Yoon HH; Noh SS; Im GI; Kim CS; Kim BS Culture on a 3,4-Dihydroxy-L-Phenylalanine-Coated Surface Promotes the Osteogenic Differentiation of Human Mesenchymal Stem Cells. Tissue Eng. Part A 2013, 19 (9–10), 1255–1263, DOI: 10.1089/ten.tea.2012.0165. [PubMed: 23237247]

(12). Rahmani M; Bidgoli SA; Rezayat SM Electrospun polymeric nanofibers for transdermal drug delivery. Nanomed. J. 2017, 4 (2), 61–70, DOI: 10.22038/nmj.2017.21210.1224.

(13). Zhuang Y; Lin KL; Yu HB Advance of Nano-Composite Electrospun Fibers in Periodontal Regeneration. Front. Chem. 2019, 7, 16, DOI: 10.3389/fchem.2019.00495. [PubMed: 30766867]

(14). Bromberg LE; Braman VM; Rothstein DM; Spacciapoli P; O'Connor SM; Nelson EJ; Buxton DK; Tonetti MS; Friden PM Sustained release of silver from periodontal wafers for treatment of periodontitis. J. Control. Release 2000, 68 (1), 63–72, DOI: 10.1016/s0168-3659(00)00233-9. [PubMed: 10884580]

(15). Candotto V; Lauritano D; Carinci F; Bignozzi CA; Pazzi D; Cura F; Severino M; Scarano A Silver-Based Chemical Device as an Adjunct of Domestic Oral Hygiene: A Study on Periodontal Patients. Materials 2018, 11 (8), 7, DOI: 10.3390/ma11081483.

(16). Cao HL; Liu XY; Meng FH; Chu PK Biological actions of silver nanoparticles embedded in titanium controlled by micro-galvanic effects. Biomaterials 2011, 32 (3), 693–705, DOI: 10.1016/j.biomaterials.2010.09.066. [PubMed: 20970183]

(17). Qin H; Cao HL; Zhao YC; Jin GD; Cheng MQ; Wang JX; Jiang Y; An ZQ; Zhang XL; Liu XY Antimicrobial and Osteogenic Properties of Silver-Ion-Implanted Stainless Steel. ACS Appl. Mater. Interfaces 2015, 7 (20), 10785–10794, DOI: 10.1021/acsami.5b01310. [PubMed: 25952114]

(18). Shao JL; Yu N; Kolwijck E; Wang B; Tan KW; Jansen JA; Walboomers XF; Yang F Biological evaluation of silver nanoparticles incorporated into chitosan-based membranes. Nanomedicine 2017, 12 (22), 2771–2785, DOI: 10.2217/nnm-2017-0172. [PubMed: 28967828]

(19). Pauksch L; Hartmann S; Rohnke M; Szalay G; Alt V; Schnettler R; Lips KS Biocompatibility of silver nanoparticles and silver ions in primary human mesenchymal stem cells and osteoblasts. Acta Biomater. 2014, 10 (1), 439–449, DOI: 10.1016/j.actbio.2013.09.037. [PubMed: 24095782]

(20). Lu ZS; Xiao J; Wang Y; Meng M In situ synthesis of silver nanoparticles uniformly distributed on polydopamine-coated silk fibers for antibacterial application. J. Colloid Interface Sci. 2015, 452, 8–14, DOI: 10.1016/j.jcis.2015.04.015. [PubMed: 25909867]

(21). Bunyaratavej P; Wang HL Collagen membranes: A review. J. Periodont. 2001, 72 (2), 215–229, DOI: 10.1902/jop.2001.72.2.215. [PubMed: 11288796]

(22). Sheikh Z; Qureshi J; Alshahrani AM; Nassar H; Ikeda Y; Glogauer M; Ganss B Collagen based barrier membranes for periodontal guided bone regeneration applications. Odontology 2017, 105 (1), 1–12, DOI: 10.1007/s10266-016-0267-0. [PubMed: 27613193]

(23). Jabbari E Osteogenic Peptides in Bone Regeneration. Curr. Pharm. Design 2013, 19 (19), 3391–3402, DOI: 10.2174/1381612811319190006.

(24). Lao LH; Zhu Y; Zhang YY; Gao ZY; Zhou F; Chen LK; Ouyang HW; Gao CY Mineralization of Collagen-Coated Electrospun Poly(lactide-co-glycolide) Nanofibrous Mesh to Enhance Growth and Differentiation of Osteoblasts and Bone Marrow Mesenchymal Stem Cells. Adv. Eng. Mater. 2012, 14 (4), B123–B137, DOI: 10.1002/adem.201180023.

(25). Li N; Chen G; Liu J; Xia Y; Chen HB; Tang H; Zhang FM; Gu N Effect of Surface Topography and Bioactive Properties on Early Adhesion and Growth Behavior of Mouse Preosteoblast MC3T3-E1 Cells. ACS Appl. Mater. Interfaces 2014, 6 (19), 17134–17143, DOI: 10.1021/am5047944. [PubMed: 25211771]

(26). Watanabe K; Petro BJ; Shlimon AE; Unterman TG Effect of periodontitis on insulin resistance and the onset of type 2 diabetes mellitus in Zucker diabetic fatty rats. J. Periodont. 2008, 79 (7), 1208–1216, DOI: 10.1902/jop.2008.070605. [PubMed: 18597603]

(27). Xue JJ; Xie JW; Liu WY; Xia YN Electrospun Nanofibers: New Concepts, Materials, and Applications. Accounts Chem. Res. 2017, 50 (8), 1976–1987, DOI: 10.1021/acs.accounts.7b00218.

(28). Ott LM; Zabel TA; Walker NK; Farris AL; Chakroff JT; Ohst DG; Johnson JK; Gehrke SH; Weatherly RA; Detamore MS Mechanical evaluation of gradient electrospun scaffolds with 3D printed ring reinforcements for tracheal defect repair. Biomed. Mater. 2016, 11 (2), 16, DOI: 10.1088/1748-6041/11/2/025020.

(29). Yang SB; Han XG; Jia YH; Zhang HB; Tang TT Hydroxypropyltrimethyl Ammonium Chloride Chitosan Functionalized-PLGA Electrospun Fibrous Membranes as Antibacterial Wound Dressing: In Vitro and In Vivo Evaluation. Polymers 2017, 9 (12), 19, DOI: 10.3390/polym9120697.

(30). Jing X; Mi HY; Wang XC; Peng XF; Turng LS Shish-Kebab-Structured Poly(epsilon-Caprolactone) Nanofibers Hierarchically Decorated with Chitosan Poly(epsilon-Caprolactone) Copolymers for Bone Tissue Engineering. ACS Appl. Mater. Interfaces 2015, 7 (12), 6955–6965, DOI: 10.1021/acsami.5b00900. [PubMed: 25761418]

(31). Chen TP; Liu TC; Su TL; Liang JF Self-Polymerization of Dopamine in Acidic Environments without Oxygen. Langmuir 2017, 33 (23), 5863–5871, DOI: 10.1021/acs.langmuir.7b01127. [PubMed: 28505456]

(32). Chen HB; Qian YZ; Xia Y; Chen G; Dai Y; Li N; Zhang FM; Gu N Enhanced Osteogenesis of ADSCs by the Synergistic Effect of Aligned Fibers Containing Collagen I. ACS Appl. Mater. Interfaces 2016, 8 (43), 29289–29297, DOI: 10.1021/acsami.6b08791. [PubMed: 27735181]

(33). Chou SF; Woodrow KA Relationships between mechanical properties and drug release from electrospun fibers of PCL and PLGA blends. J. Mech. Behav. Biomed. Mater. 2017, 65, 724–733, DOI: 10.1016/j.jmbbm.2016.09.004. [PubMed: 27756048]

(34). Yang K; Lee JS; Kim J; Lee YB; Shin H; Um SH; Kim JB; Park KI; Lee H; Cho SW Polydopamine-mediated surface modification of scaffold materials for human neural stem cell engineering. Biomaterials 2012, 33 (29), 6952–6964, DOI: 10.1016/j.biomaterials.2012.06.067. [PubMed: 22809643]

(35). He W; Elkhooly TA; Liu XJ; Cavallaro A; Taheri S; Vasilev K; Feng QL Silver nanoparticle based coatings enhance adipogenesis compared to osteogenesis in human mesenchymal stem cells through oxidative stress. J. Mat. Chem. B 2016, 4 (8), 1466–1479, DOI: 10.1039/c5tb02482j.

(36). Teixeira BN; Aprile P; Mendonca RH; Kelly DJ; Thire R Evaluation of bone marrow stem cell response to PLA scaffolds manufactured by 3D printing and coated with polydopamine and type I collagen. J. Biomed. Mater. Res. Part B 2019, 107 (1), 37–49, DOI: 10.1002/jbm.b.34093.

(37). Chen KL; Xie KN; Long Q; Deng LJ; Fu ZQ; Xiao HH; Xie L Fabrication of core-shell Ag@pDA@HAp nanoparticles with the ability for controlled release of Ag+ and superior hemocompatibility. RSC Adv. 2017, 7 (47), 29368–29377, DOI: 10.1039/c7ra03494f.

(38). Ning CY; Wang XL; Li LH; Zhu Y; Li M; Yu P; Zhou L; Zhou ZN; Chen JQ; Tan GX; Zhang Y; Wang YJ; Mao CB Concentration Ranges of Antibacterial Cations for Showing the Highest Antibacterial Efficacy but the Least Cytotoxicity against Mammalian Cells: Implications for a New Antibacterial Mechanism. Chem. Res. Toxicol. 2015, 28 (9), 1815–1822, DOI: 10.1021/acs.chemrestox.5b00258. [PubMed: 26258952]

(39). Zhou WH; Jia ZJ; Xiong P; Yan JL; Li YY; Li M; Cheng Y; Zhenie YF Bioinspired and Biomimetic AgNPs/Gentamicin-Embedded Silk Fibroin Coatings for Robust Antibacterial and Osteogenetic Applications. ACS Appl. Mater. Interfaces 2017, 9 (31), 25830–25846, DOI: 10.1021/acsami.7b06757. [PubMed: 28731325]

(40). Ismail YMB; Ferreira AM; Bretcanu O; Dalgarno K; El Haj AJ Polyelectrolyte multi-layers assembly of SiCHA nanopowders and collagen type I on aminolysed PLA films to enhance cell-material interactions. Colloid Surf. B-Biointerfaces 2017, 159, 445–453, DOI: 10.1016/j.colsurfb.2017.07.086.

(41). Chantre CO; Campbell PH; Golecki HM; Buganza AT; Capulli AK; Deravi LF; Dauth S; Sheehy SP; Paten JA; Gledhill K; Doucet YS; Abaci HE; Ahn S; Pope BD; Ruberti JW; Hoerstrup SP; Christiano AM; Parker KK Production-scale fibronectin nanofibers promote wound closure and tissue repair in a dermal mouse model. Biomaterials 2018, 166, 96–108, DOI: 10.1016/j.biomaterials.2018.03.006. [PubMed: 29549768]

(42). Anselme K; Ponche A; Bigerelle M Relative influence of surface topography and surface chemistry on cell response to bone implant materials. Part 2: biological aspects. Proc. Inst. Mech. Eng. Part H-J. Eng. Med. 2010, 224 (H12), 1487–1507, DOI: 10.1243/09544119jeim901.

(43). Siebers MC; ter Brugge PJ; Walboomers XF; Jansen JA Integrins as linker proteins between osteoblasts and bone replacing materials. A critical review. Biomaterials 2005, 26 (2), 137–146, DOI: 10.1016/j.biomaterials.2004.02.021. [PubMed: 15207460]

(44). Popova SN; Lundgren-Akerlund E; Wiig H; Gullberg D Physiology and pathology of collagen receptors. Acta Physiol. 2007, 190 (3), 179–187, DOI: 10.1111/j.1748-1716.2007.01718.x.

(45). Sun YH; Deng Y; Ye ZY; Liang SS; Tang ZH; Wei SC Peptide decorated nano-hydroxyapatite with enhanced bioactivity and osteogenic differentiation via polydopamine coating. Colloid Surf. B-Biointerfaces 2013, 111, 107–116, DOI: 10.1016/j.colsurfb.2013.05.037.

(46). Ku SH; Ryu J; Hong SK; Lee H; Park CB General functionalization route for cell adhesion on non-wetting surfaces. Biomaterials 2010, 31 (9), 2535–2541, DOI: 10.1016/j.biomaterials.2009.12.020. [PubMed: 20061015]

(47). Carracedo S; Lu N; Popova SN; Jonsson R; Eckes B; Gullberg D The Fibroblast Integrin alpha 11 beta 1 Is Induced in a Mechanosensitive Manner Involving Activin A and Regulates Myofibroblast Differentiation. J. Biol. Chem. 2010, 285 (14), 10434–10445, DOI: 10.1074/jbc.M109.078766. [PubMed: 20129924]

(48). Tiger CF; Fougerousse F; Grundstrom G; Velling T; Gullberg D alpha 11 beta 1 integrin is a receptor for interstitial collagens involved in cell migration and collagen reorganization on

mesenchymal nonmuscle cells. Dev. Biol. 2001, 237 (1), 116–129, DOI: 10.1006/dbio.2001.0363. [PubMed: 11518510]

(49). Qing T; Mahmood M; Zheng YT; Biris AS; Shi LM; Casciano DA A genomic characterization of the influence of silver nanoparticles on bone differentiation in MC3T3-E1 cells. J. Appl. Toxicol. 2018, 38 (2), 172–179, DOI: 10.1002/jat.3528. [PubMed: 28975650]

(50). Deligianni DD; Katsala ND; Koutsoukos PG; Missirlis YF Effect of surface roughness of hydroxyapatite on human bone marrow cell adhesion, proliferation, differentiation and detachment strength. Biomaterials 2001, 22 (1), 87–96, DOI: 10.1016/s0142-9612(00)00174-5. [PubMed: 11085388]

(51). Bruderer M; Richards RG; Alini M; Stoddart MJ ROLE AND REGULATION OF RUNX2 IN OSTEOGENESIS. Eur. Cells Mater. 2014, 28, 269–286, DOI: 10.22203/eCM.v028a19.

(52). Sun J; Li JY; Li CC; Yu YC Role of bone morphogenetic protein-2 in osteogenic differentiation of mesenchymal stem cells. Mol. Med. Rep. 2015, 12 (3), 4230–4237, DOI: 10.3892/mmr.2015.3954. [PubMed: 26096280]

(53). Wei M; Li S; Le WD Nanomaterials modulate stem cell differentiation: biological interaction and underlying mechanisms. J. Nanobiotechnol. 2017, 15, 13, DOI: 10.1186/s12951-017-0310-5.

(54). Liu XJ; He W; Fang Z; Kienzle A; Feng QL Influence of Silver Nanoparticles on Osteogenic Differentiation of Human Mesenchymal Stem Cells. J. Biomed. Nanotechnol. 2014, 10 (7), 1277–1285, DOI: 10.1166/jbn.2014.1824. [PubMed: 24804548]

(55). Mahmood M; Li ZG; Casciano D; Khodakovskaya MV; Chen T; Karmakar A; Dervishi E; Xu Y; Mustafa T; Watanabe F; Fejleh A; Whitlow M; Al-Adami M; Ghosh A; Biris AS Nanostructural materials increase mineralization in bone cells and affect gene expression through miRNA regulation. J. Cell. Mol. Med. 2011, 15 (11), 2297–2306, DOI: 10.1111/j.1582-4934.2010.01234.x. [PubMed: 21143388]

(56). Cao HL; Zhang WJ; Meng FH; Guo JS; Wang DH; Qian S; Jiang XQ; Liu XY; Chu PK Osteogenesis Catalyzed by Titanium-Supported Silver Nanoparticles. ACS Appl. Mater. Interfaces 2017, 9 (6), 5149–5157, DOI: 10.1021/acsami.6b15448. [PubMed: 28111942]

(57). McKee C; Chaudhry GR Advances and challenges in stem cell culture. Colloid Surf. B-Biointerfaces 2017, 159, 62–77, DOI: 10.1016/j.colsurfb.2017.07.051.

(58). Cheng YX; Ramos D; Lee P; Liang DN; Yu XJ; Kumbar SG Collagen Functionalized Bioactive Nanofiber Matrices for Osteogenic Differentiation of Mesenchymal Stem Cells: Bone Tissue Engineering. J. Biomed. Nanotechnol. 2014, 10 (2), 287–298, DOI: 10.1166/jbn.2014.1753. [PubMed: 24738337]

(59). George J; Kuboki Y; Miyata T Differentiation of mesenchymal stem cells into osteoblasts on honeycomb collagen scaffolds. Biotechnol. Bioeng. 2006, 95 (3), 404–411, DOI: 10.1002/bit.20938. [PubMed: 16572435]

(60). Fensky F; Reichert JC; Traube A; Rackwitz L; Siebenlist S; Noth U Chondrogenic predifferentiation of human mesenchymal stem cells in collagen type I hydrogels. Biomed. Eng.-Biomed. Tech. 2014, 59 (5), 375–383, DOI: 10.1515/bmt-2013-0076.

(61). Lin YL; Chen CP; Lo CM; Wang HS Stiffness-controlled three-dimensional collagen scaffolds for differentiation of human Wharton's jelly mesenchymal stem cells into cardiac progenitor cells. J. Biomed. Mater. Res. Part A 2016, 104 (9), 2234–2242, DOI: 10.1002/jbm.a.35762.

(62). Xia LG; Lin KL; Jiang XQ; Xu YJ; Zhang ML; Chang J; Zhang ZY Enhanced osteogenesis through nano-structured surface design of macroporous hydroxyapatite bioceramic scaffolds via activation of ERK and p38 MAPK signaling pathways. J. Mat. Chem. B 2013, 1 (40), 5403–5416, DOI: 10.1039/c3tb20945h.

(63). Marques SM; Rico P; Carvalho I; Ribelles JLG; Fialho L; Lanceros-Mendez S; Henriques M; Carvalho S MC3T3-E1 Cell Response to Ti1-xAgx and Ag-TiNx Electrodes Deposited on Piezoelectric Poly(vinylidene fluoride) Substrates for Sensor Applications. ACS Appl. Mater. Interfaces 2016, 8 (6), 4199–4207, DOI: 10.1021/acsami.5b11922. [PubMed: 26840928]

(64). Yu XH; Walsh J; Wei M Covalent immobilization of collagen on titanium through polydopamine coating to improve cellular performances of MC3T3-E1 cells. RSC Adv. 2014, 4 (14), 7185–7192, DOI: 10.1039/c3ra44137g.

(65). Zhang XF; Liu ZG; Shen W; Gurunathan S Silver Nanoparticles: Synthesis, Characterization, Properties, Applications, and Therapeutic Approaches. Int. J. Mol. Sci. 2016, 17 (9), 34, DOI: 10.3390/ijms17091534.

(66). Chmielewska DK; Sartowska B; Starosta W; Walo M Radiation synthesis of silver nano- and microparticles in cellulose fibers. Nukleonika 2010, 55 (3), 345–349.

(67). Quinteros MA; Aristizabal VC; Dalmasso PR; Paraje MG; Paez PL Oxidative stress generation of silver nanoparticles in three bacterial genera and its relationship with the antimicrobial activity. Toxicol. Vitro 2016, 36, 216–223, DOI: 10.1016/j.tiv.2016.08.007.

(68). Loza K; Diendorf J; Sengstock C; Ruiz-Gonzalez L; Gonzalez-Calbet JM; Vallet-Regi M; Koller M; Epple M The dissolution and biological effects of silver nanoparticles in biological media. J. Mat. Chem. B 2014, 2 (12), 1634–1643, DOI: 10.1039/c3tb21569e.

(69). Tran QH; Nguyen VQ; Le AT Silver nanoparticles: synthesis, properties, toxicology, applications and perspectives. Adv. Nat. Sci.-Nanosci Nanotechnol 2013, 4 (3), 20, DOI: 10.1088/2043-6262/4/3/033001.

(70). Greulich C; Braun D; Peetsch A; Diendorf J; Siebers B; Epple M; Koller M The toxic effect of silver ions and silver nanoparticles towards bacteria and human cells occurs in the same concentration range. RSC Adv. 2012, 2 (17), 6981–6987, DOI: 10.1039/c2ra20684f.

(71). Mombelli A; Zappa U; Bragger U; Lang NP Systemic antimicrobial treatment and guided tissue regeneration - Clinical and microbiological effects in furcation defects. J. Clin. Periodontol. 1996, 23 (4), 386–396, DOI: 10.1111/j.1600-051X.1996.tb00562.x. [PubMed: 8739172]

(72). Kornman KS; Robertson PB Fundamental principles affecting the outcomes of therapy for osseous lesions. Periodontol. 2000 2000, 22, 22–43, DOI: 10.1034/j.1600-0757.2000.2220103.x. [PubMed: 11276514]

(73). Yao QQ; Cosme JGL; Xu T; Miszuk JM; Picciani PHS; Fong H; Sun HL Three dimensional electrospun PCL/PLA blend nanofibrous scaffolds with significantly improved stem cells osteogenic differentiation and cranial bone formation. Biomaterials 2017, 115, 115–127, DOI: 10.1016/j.biomaterials.2016.11.018. [PubMed: 27886552]

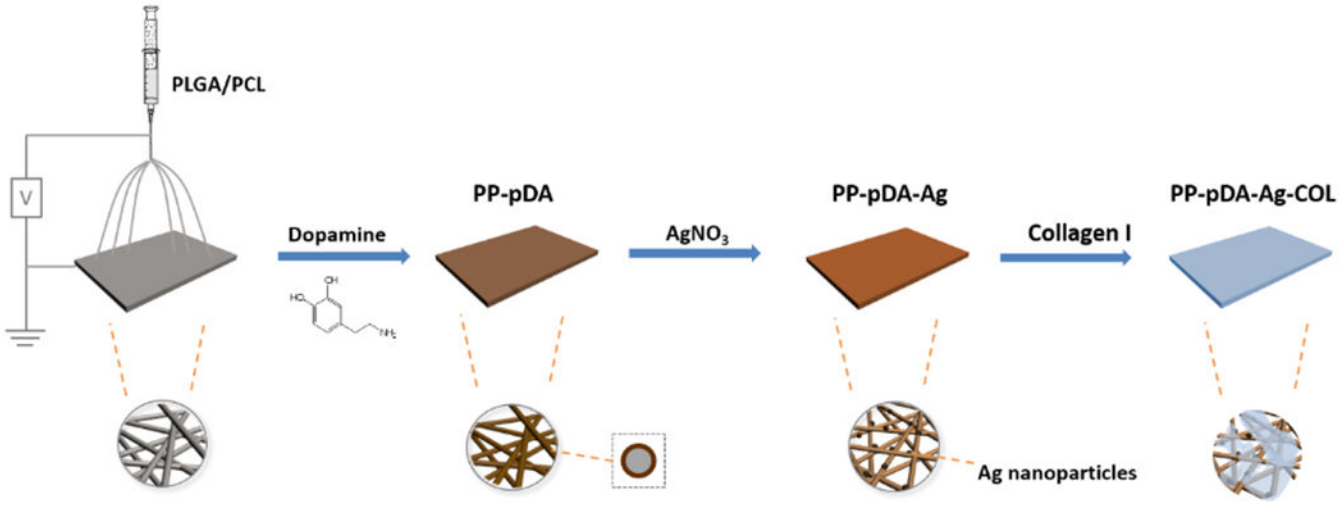

Figure 1.

Schematic illustration of the preparation procedure of PP-pDA-Ag-COL scaffolds. PLGA/PCL scaffolds were prepared by electrospun technology. Ag nanoparticles were in site reduced by polydopamine, and then coated by collagen I.

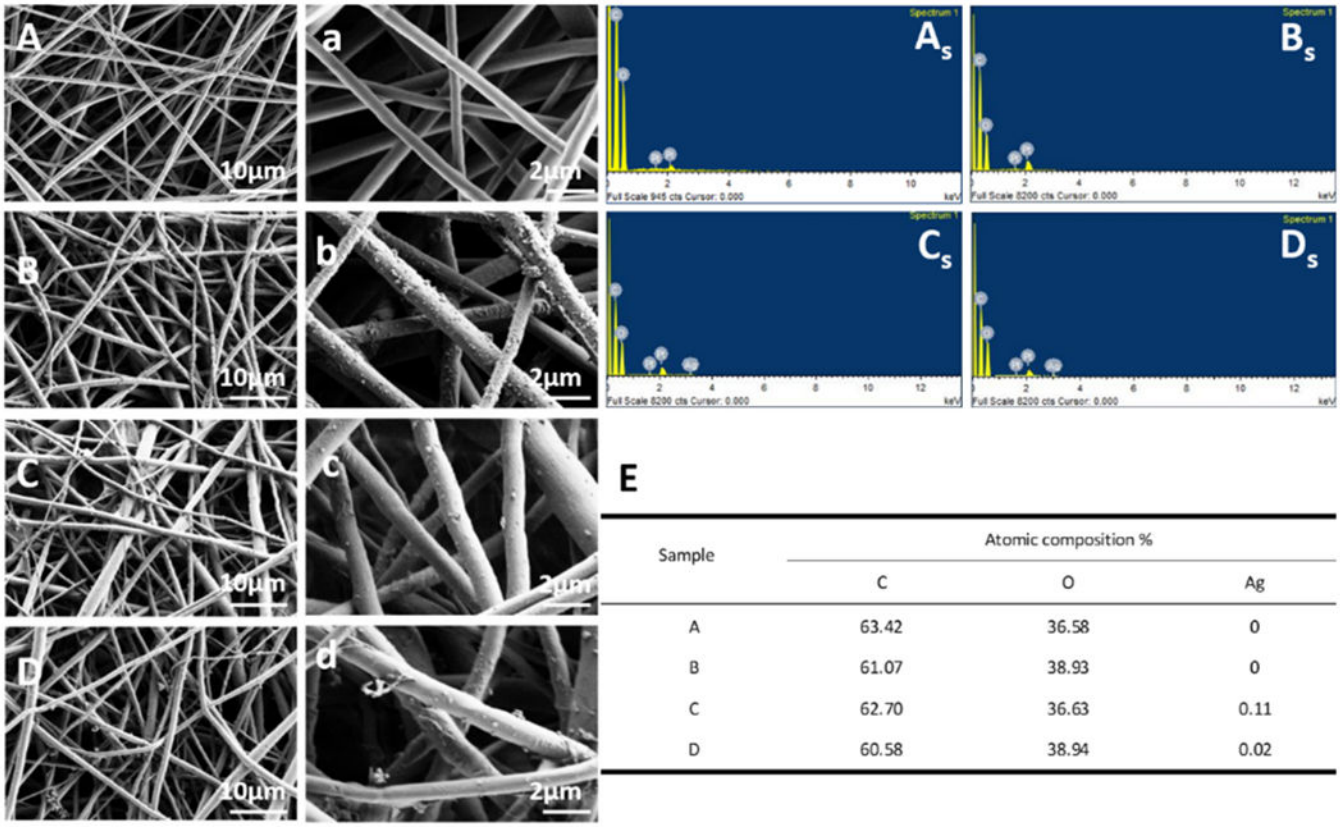

E

Sample	Atomic composition %		
	C	O	Ag
A	63.42	36.58	0
B	61.07	38.93	0
C	62.70	36.63	0.11
D	60.58	38.94	0.02

Figure 2.

Structure and composition of the PP-pDA-Ag-COL and control scaffolds. (A, a- D, d) SEM images of the PP (A, a), PP-pDA (B, b), PP-pDA-Ag (C, c) and PP-pDA-Ag-COL (D, d) scaffolds at lower (A, B, C and D) and higher (a, b, c and d) magnification. Note that all four scaffolds exhibited unique 3D architectures with interconnected randomly-oriented nanofibers and mimicked the arrangement of native extracellular matrices. (As-Ds) EDX spectrum of the PP (A_s), PP-pDA (B_s), PP-pDA-Ag (C_s) and PP-pDA-Ag-COL (D_s) scaffolds, and (E) elemental composition of the scaffold surfaces C-Carbon, O-Oxygen, Ag-Silver.

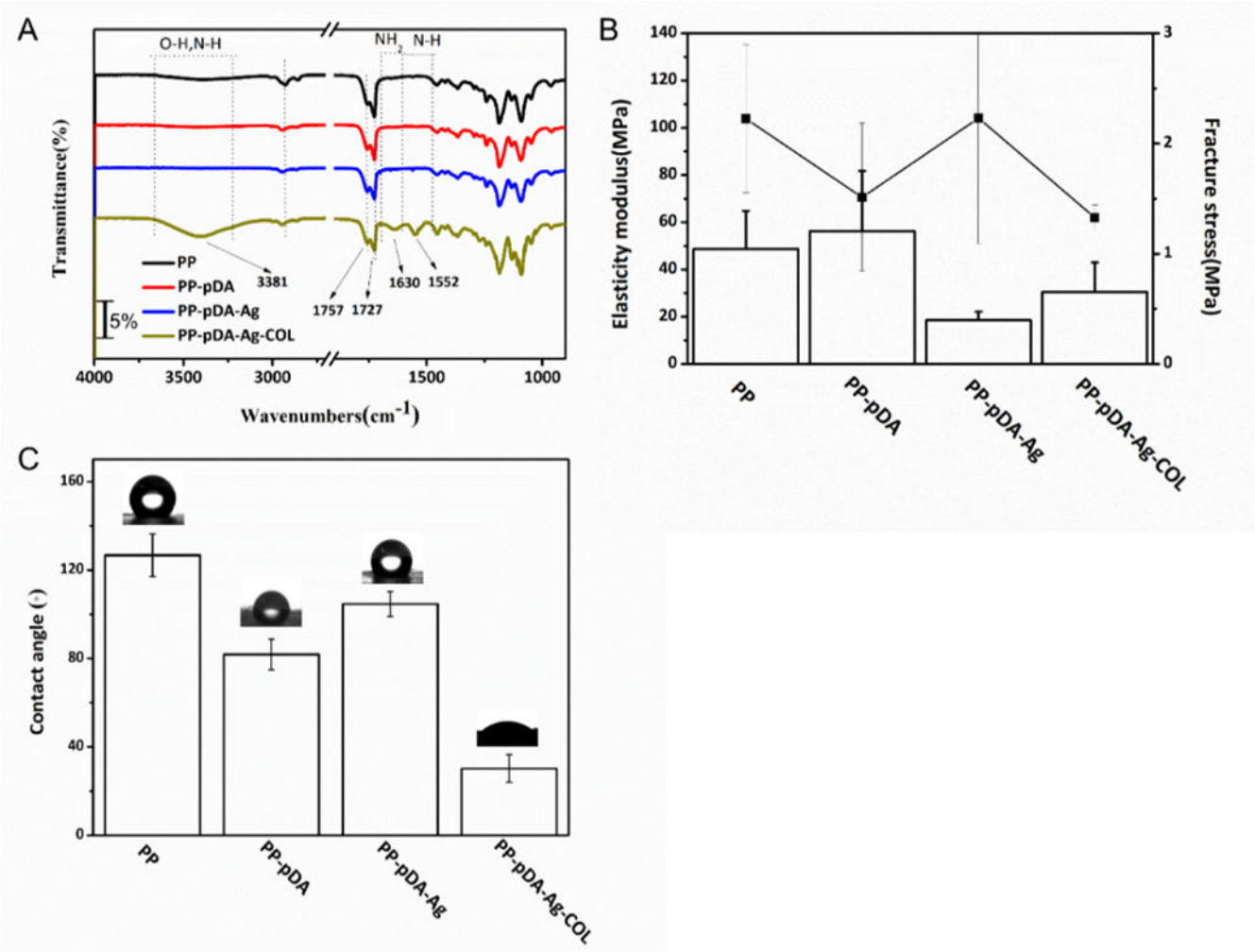

Figure 3.

Physicochemical and mechanical properties of the PP-pDA-Ag-COL and control scaffolds. (A). FT-IR spectra of the PP, PP-pDA, PP-pDA-Ag and PP-pDA-Ag-COL scaffolds. (B). Mechanical properties of tensile strength and elastic modulus of the PP, PP-pDA, PP-pDA-Ag and PP-pDA-Ag-COL scaffolds. The elastic modulus (left Y axis) is compared among the four scaffolds by column chart while the tensile strength (right Y axis) is compared by the line chart. (C). Contact angle of the PP, PP-pDA, PP-pDA-Ag and PP-pDA-Ag-COL scaffolds. The images above each column illustrate the actual contact angle when water drops onto the scaffolds. Note the significantly lower contact angle of the PP-pDA-Ag-COL scaffold, indicative of better hydrophilic properties than the three control scaffolds.

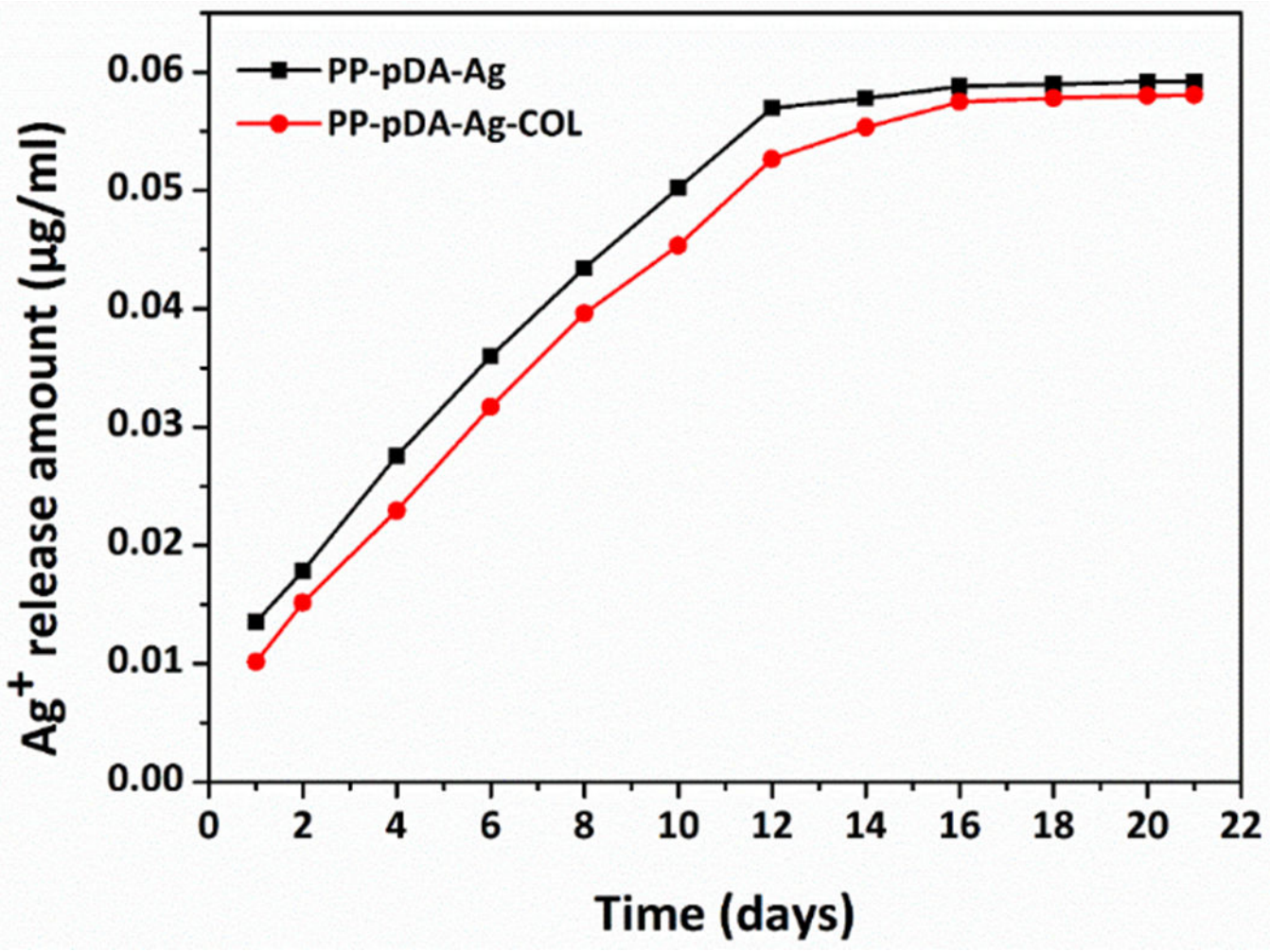

Figure 4.

Cumulative Ag^+ release from two silver-modified scaffolds, PP-pDA-Ag and PP-pDA-Ag-COL. Silver ions were accumulatively and steadily released from PP-pDA-Ag and PP-pDA-Ag-COL and measured at 1, 2, 4, 6, 8, 10, 12, 14, 16, 18, 20 and 21 days in PBS buffer. Note that PP-pDA-Ag and PP-pDA-Ag-COL showed similar release curves while the PP-pDA-Ag-COL scaffold had slightly slower release rate.

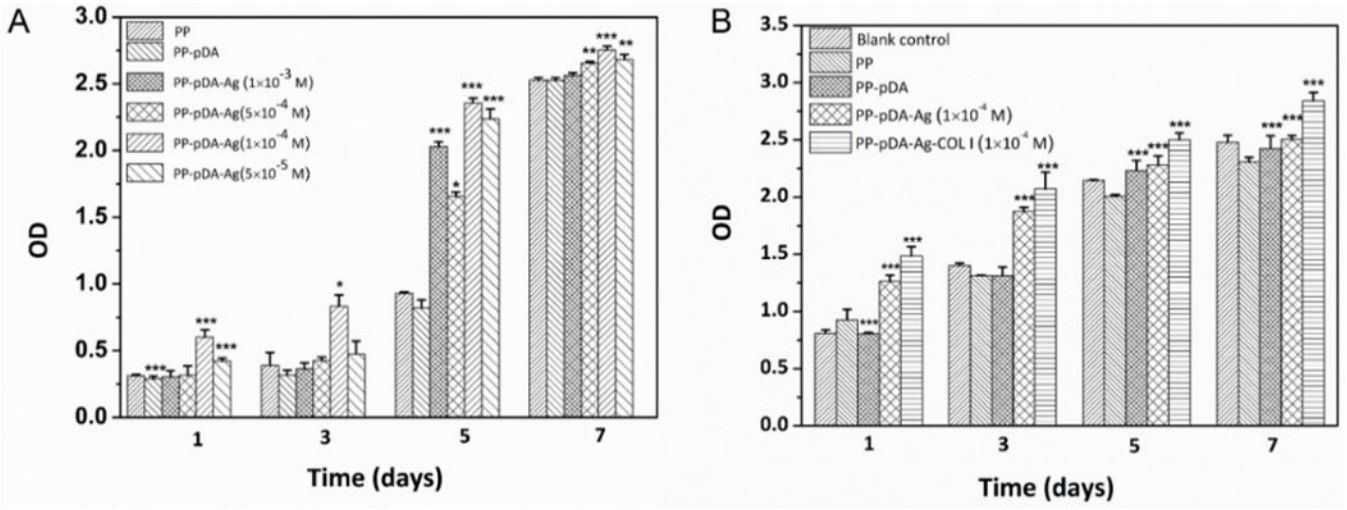

Figure 5.

The effect of the PP-pDA-Ag-COL and control scaffolds on cell proliferation. MC3T3 cells were seeded onto the PP, PP-pDA and $AgNO_3$ coated PP-pDA-Ag scaffolds at concentrations of 5×10^{-5}, 1×10^{-4}, 5×10^{-4} and 1×10^{-3}M (A), or the cells were cultured on the PP, PP-pDA, PP-pDA-Ag (10^{-4}M) and PP-pDA-Ag-COL (10^{-4}M) scaffolds (B) for 1, 3, 5 and 7 days. Cell viability and proliferation was determined as OD value and compared with PP using a CCK-8 kit. * $p < 0.05$, ** $p < 0.01$, *** $p < 0.001$.

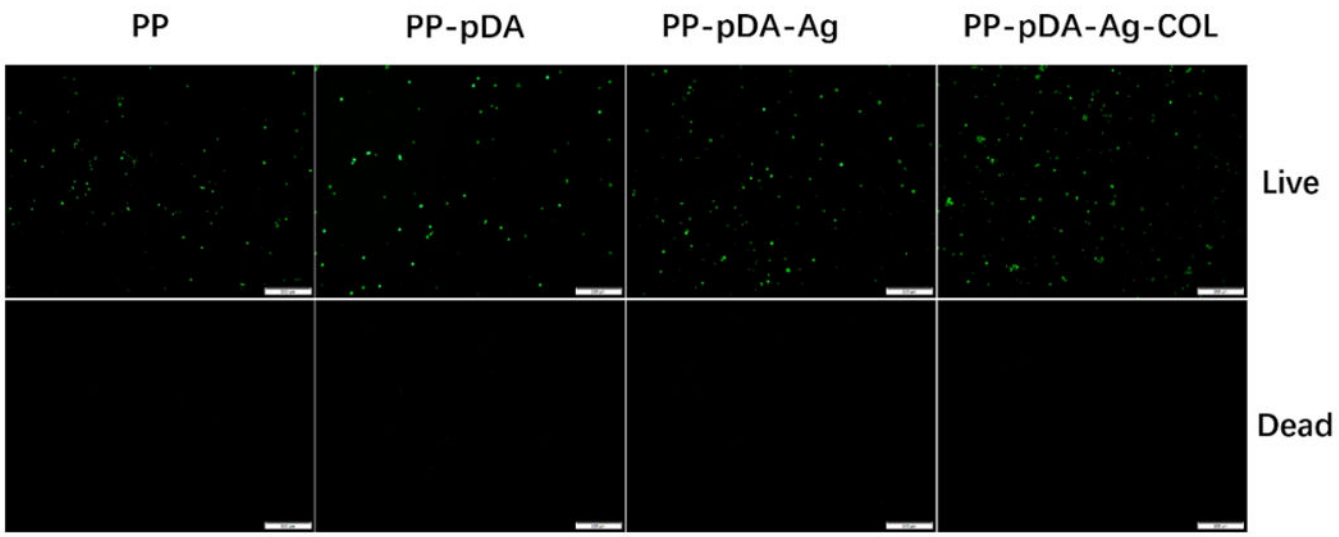

Figure 6.

Fluorescent images of live/dead staining of MC3T3-E1 on scaffolds after culturing for 3 days. Scale bar is 500μm. Live cells were stained in green while dead cells were stained in red.

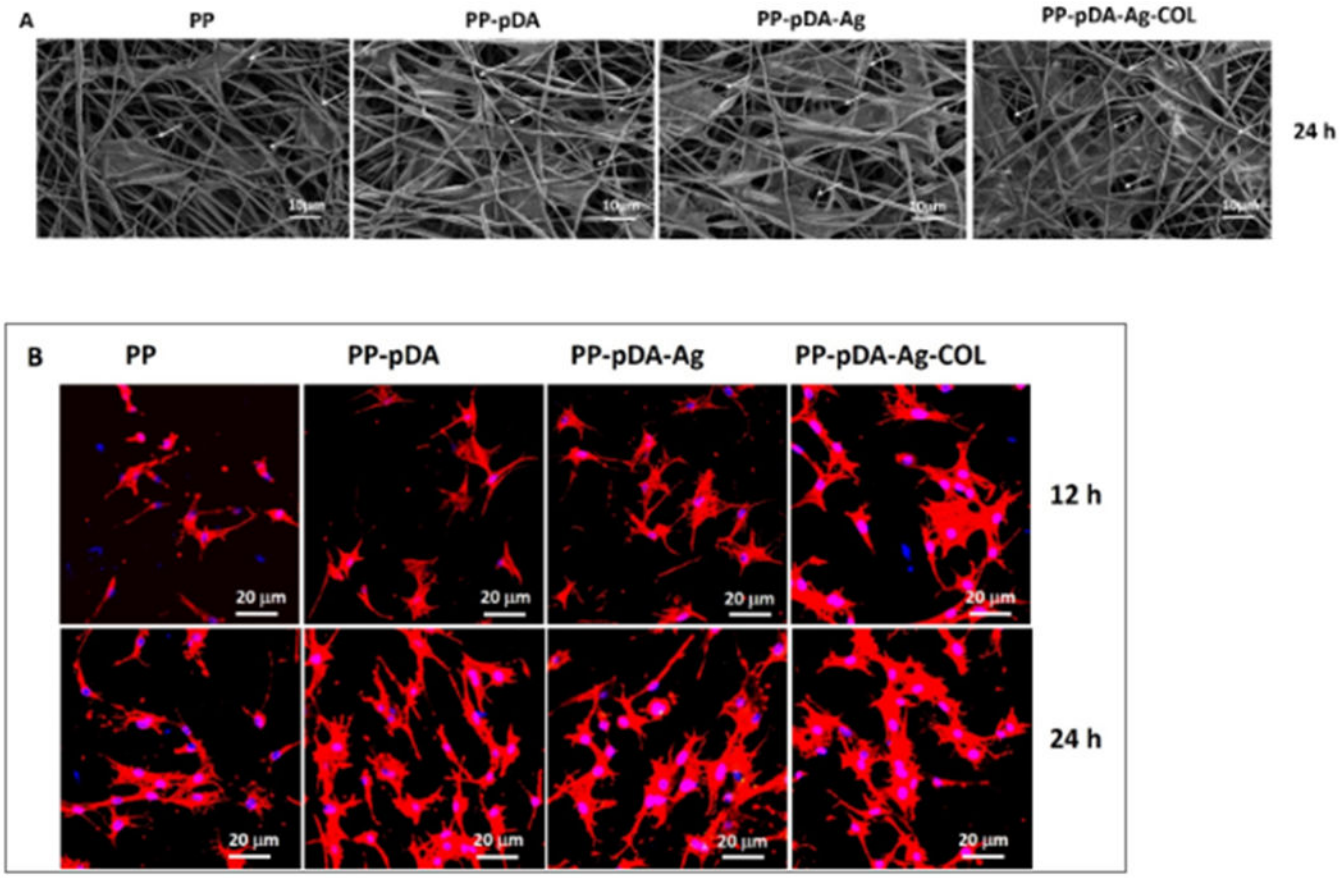

Figure 7.

Cell morphology and attachment on the PP-pDA-Ag-COL and control scaffolds. MC3T3 cells were cultured on the PP, PP-pDA, PP-pDA-Ag and PP-pDA-Ag-COL scaffolds for 12h or 24h. (A) FESEM images of the scaffolds with cultured cells for 24h. The arrowheads point to the attached and spread cells on the scaffolds. (B) Fluorescent staining of cytoskeleton after the cells were cultured for 12h and 24h. Note that the MC3T3 cells on the PP-pDA-Ag-COL scaffold had higher cell density and were well spread.

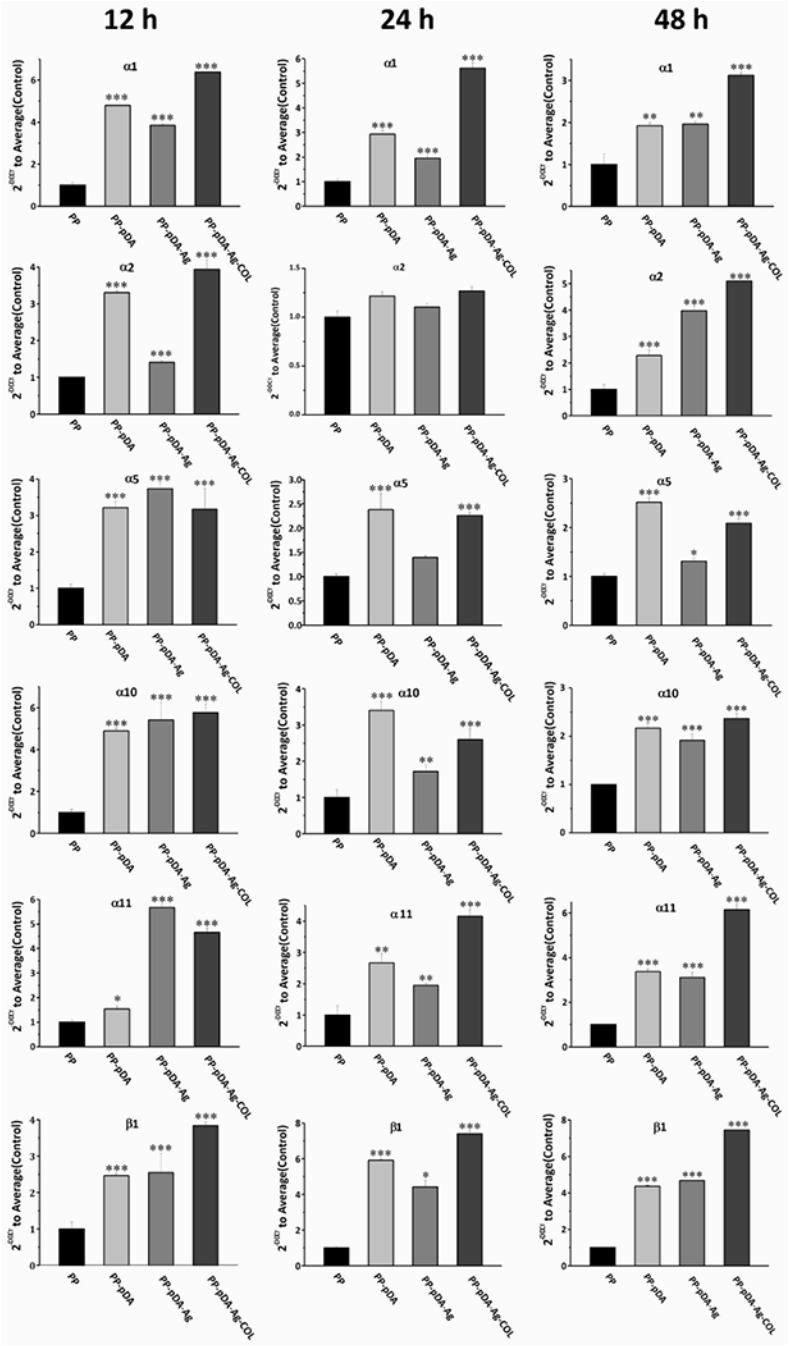

Figure 8.

Integrins β1, α1, α2, α5, α10, α11 expression in MC3T3 cells cultured on PP, PP-pDA, PP-pDA-Ag and PP-pDA-Ag-COL scaffolds for 12h, 24h and 48h. The expression of target genes was normalized to GAPDH and the relative expression level was calculated by the $2^{-\Delta\Delta Ct}$ method. * $p < 0.05$, ** $p < 0.01$, *** $p < 0.001$, compare with PP.

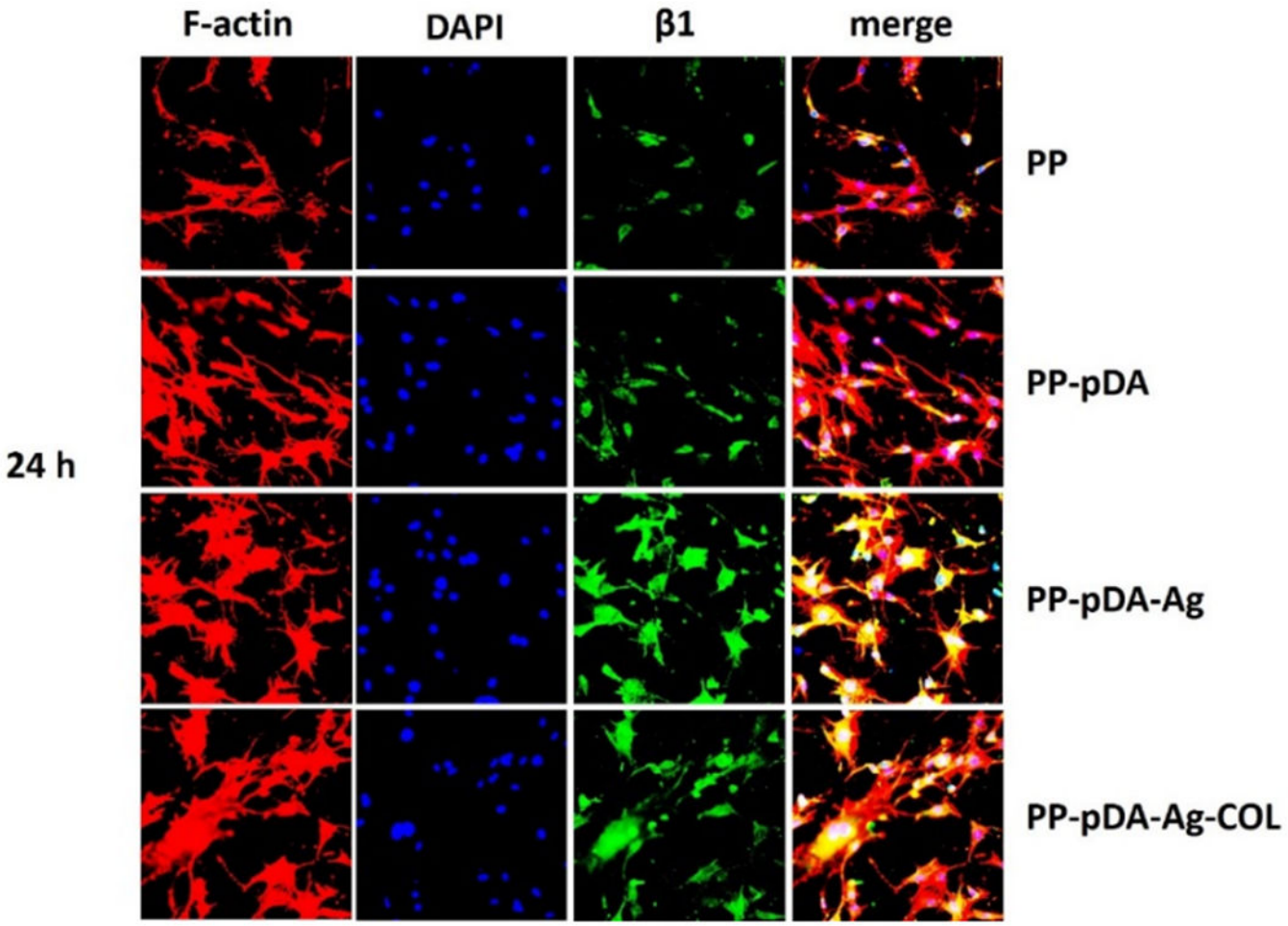

Figure 9.

Integrin β1 expression in MC3T3 cells cultured on PP-pDA-Ag-COL and control scaffolds. MC3T3 cells were cultured on the scaffolds for 24 h and then fluorescently labeled for F-actin (red) or for integrin β1 via immunofluorescence (green). Note the increased levels of integrin β1 on the MC3T3 cells on the PP-pDA-Ag-COL scaffold.

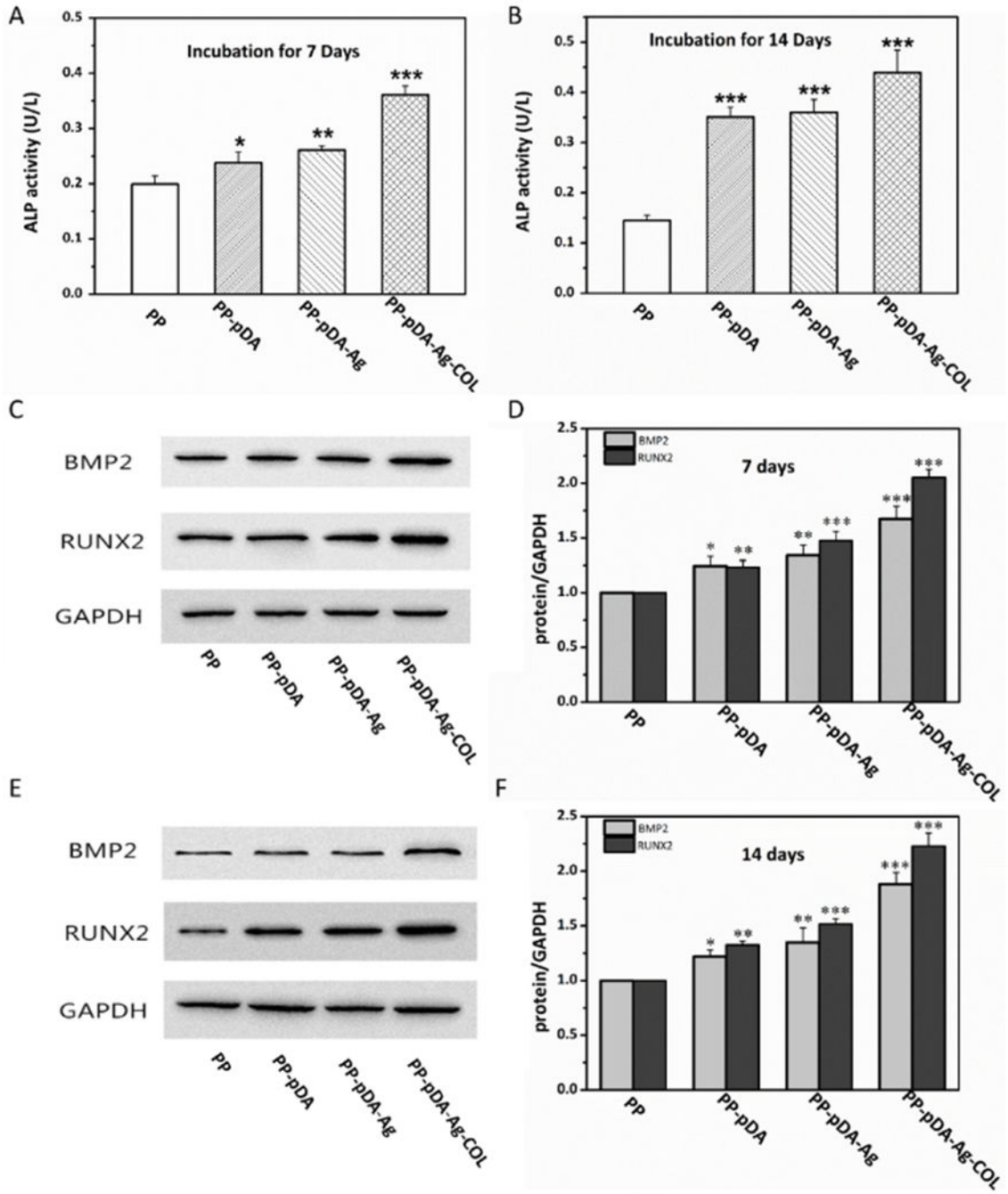

Figure 10.

Effects of the PP-pDA-Ag-COL and control scaffolds on osteogenic differentiation of MC3T3 cells. Cells were cultured on the scaffolds for 7 (A, C, D) or 14 (B, E, F) days. (A, B) ALP activity was determined using an alkaline phosphatase assay kit and normalized to the total protein content. The protein expression of BMP2 and RUNX2 for 7 (C, D) and 14 (E, F) days was determined by Western blotting. The expression levels were calculated by densitometry analysis relative to GAPDH. * $p < 0.05$, ** $p < 0.01$, *** $p < 0.001$, compare with PP.

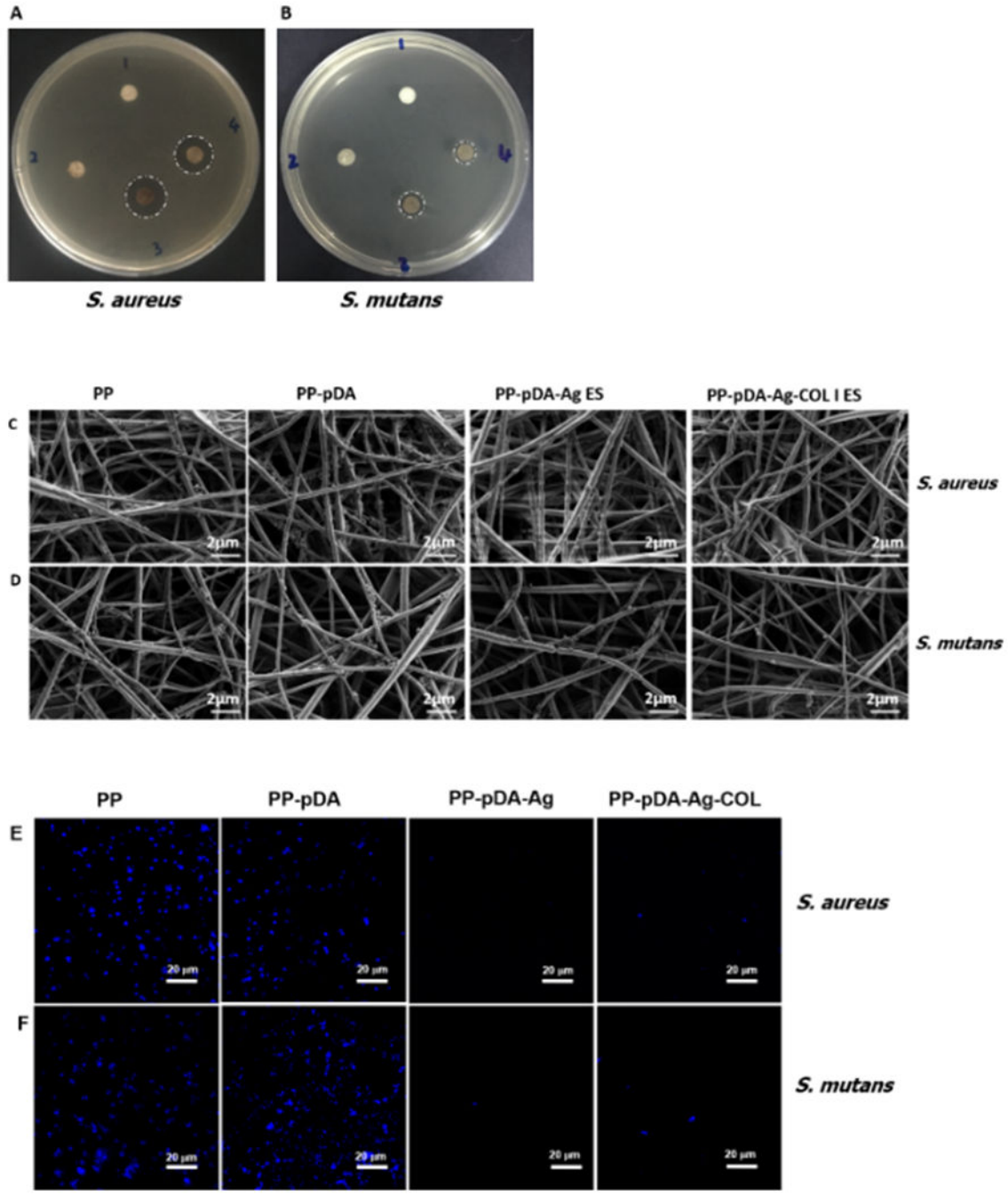

Figure 11.

Antibacterial properties of the PP-pDA, PP-pDA-Ag and PP-pDA-Ag-COL scaffolds. (A, B) Agar diffusion tests. Bacteria *S. aureus* (A) and *S. mutans* (B) were inoculated in LB agar (A) or Brian Heart Infusion agar (B). The PP (#1), PP-pDA (#2), PP-pDA-Ag (#3) and PP-pDA-Ag-COL (#4) scaffolds were punched into 6 mm disks and placed on the surface of the agars. The plates were incubated for 24 h. The circles point to the diameter of the inhibition zone (DIZ). (C-F) Bacterial attachment on the scaffolds. The PP, PP-pDA, PP-pDA-Ag and PP-pDA-Ag-COL scaffolds were incubated with *S. aureu* and *S. mutans* suspension at 37 °C

for 24h and then dehydrated. Surface topography and antibacterial ability of the scaffolds was observed by FESEM (C, D). Scar bar= 2 μm. Bacterial fluorescence (E, F) was captured by CLSM after the bacteria were stained with DAPI. Scar bar= 20 μm.

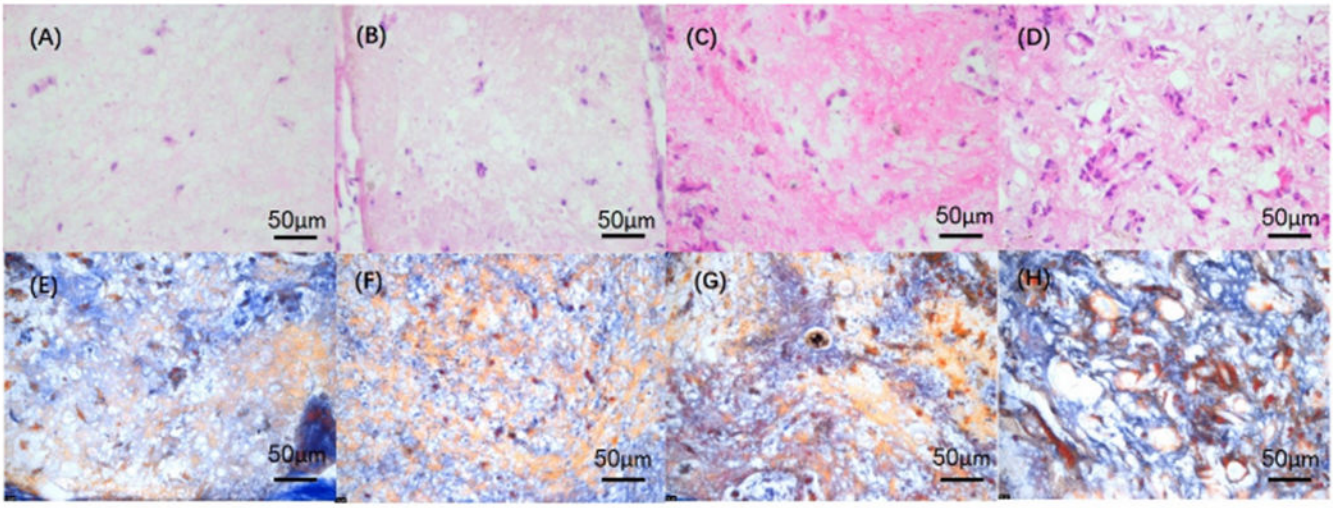

Figure 12.

Subcutaneous implantation of PP-pDA-Ag-COL and three control scaffolds. (A-D) H&E staining. Note that much more cells penetrated into PP-pDA-Ag-COL (D) scaffolds than PP (A), PP-pDA (B), PP-pDA-Ag (C) scaffolds, indicating that PP-pDA-Ag-COL had better biocompatibility and biomimetic capacity to accommodate cell recruitment. (E-H) Mallory's Trichrome staining. Collagen fibers, reticulum and mucous shades were stained in blue, elastic fibers in pink, yellow or unstained, muscle, alpha and beta cells in blue and nuclei in red.

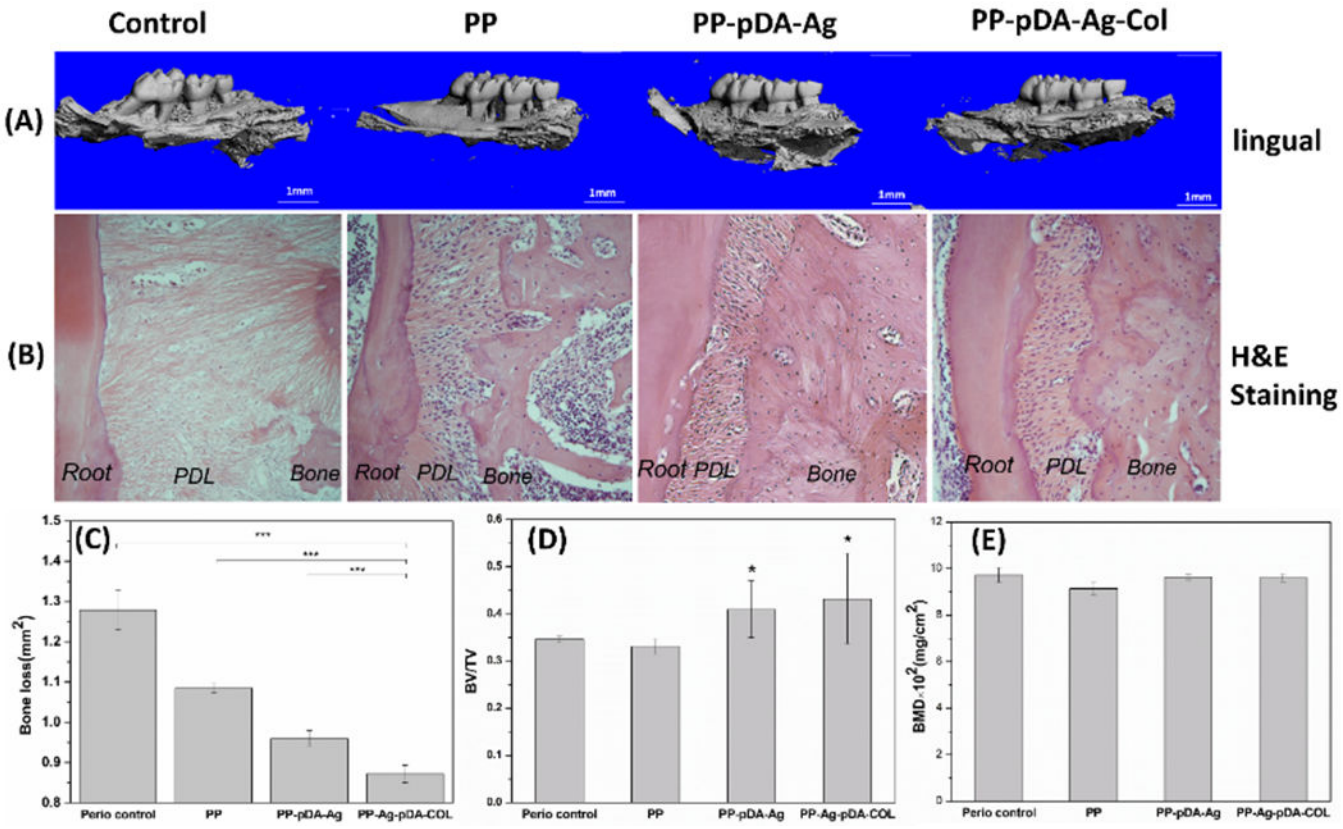

Figure 13.

Effect of our PP-pDA-Ag-COL scaffold on periodontal status following implantation in a periodontitis mouse model. (A) μCT 3D reconstruction of the left maxillary mouse molars after 6-week implantation of PP, PP-pDA-Ag and PP-pDA-Ag-COL scaffolds subjected to GTR treatment. The blank control is the periodontitis mouse model. (B) H&E staining of the regenerated periodontal tissues after 6-week implantation of PP, PP-pDA-Ag and PP-pDA-Ag-COL scaffolds subjected to GTR treatment. The periodontitis mouse model is the control. (C) Alveolar bone loss of the maxillary mouse molars in periodontitis control, PP, PP-pDA-Ag and PP-pDA-Ag-COL. (D) The bone volume in periodontitis control, PP, PP-pDA-Ag and PP-pDA-Ag-COL. (E) Bone mineral density of the alveolar bone in periodontitis control, PP, PP-pDA-Ag and PP-pDA-Ag-COL. * $p < 0.05$, *** $p < 0.001$ multiple compare. There was significantly less bone loss in the PP-pDA-Ag-COL scaffold group, suggesting that the local release of AgNPs delivered by the novel scaffolds PP-pDA-Ag-COL via GTR treatments contributed to the alleviation of periodontal inflammation and facilitated bone regeneration in a periodontitis mouse model.

Table 1.

Sequences of Primers Used in the Study.

Gene	Forward primer (5′-3′)	Reverse primer (5′-3′)
α1 Integrin	CTGCTGCCTGTGGACTTTAG	CTGGAGCGGTGGAAGAGTAA
α2 Integrin	GGGACCTCACAAACACCTTC	ACTGCTATGCCGAACCTCAG
α5 Integrin	GGGAGTGAGACCTGGCAACT	CTGGAGCGGTGGAAGAGTAA
α10 Integrin	TTGTGAGAGCAGCAAGGAAC	TAGTGACCAAGGACCGCAAT
α11 Integrin	AGGATGGGCTTGTGGACCTA	GACGGTTGCTGTTTGGAAGT
β1 Integrin	ATCCCAATTGTAGCAGGCGTGGTT	GACCACAGTTGTCACGGCACTC
gapdh	CCTTCCGTGTTCCTACCC	CAACCTGGTCCTCAGTGTAG